Article published online: 2023-09-19

Fatty Liver Disease: Pathophysiology and Imaging Features

Sharad Maheshwari[1] Sachin Kumar[2] Bharatbhai V. Nakshiwala[1] Ayush Srivastav[1] Vinaya Chavan[1] Abhijit Raut[1] Anoushka Maheshwari[3]

[1] Department of Radiology, Kokilaben Hospital, Andheri West, Mumbai, Maharashtra, India
[2] Department of Radiology, Ruban Memorial Hospital, Patna, Bihar, India
[3] Department of Oncology, Kokilaben Hospital, Andheri West, Mumbai, Maharashtra, India

Address for correspondence Sharad Maheshwari, MBBS, MD, Department of Radiology, Kokilaben Hospital, Andheri West, Mumbai 400053, Maharashtra, India (e-mail: sharaddoc@gmail.com).

Indographics 2022;1:57–77.

Abstract

Fatty liver is a benign condition to start with and is characterized by excess triglyceride in the hepatocytes. However, in the long term, it can lead to increased oxidative stress & inflammation, with resultant steatohepatitis. This can subsequently progress to cirrhosis and eventually an increased risk of developing hepatocellular carcinoma (HCC). Liver biopsy is the gold standard for quantification of fat and assessing the degree of fibrosis, however, it is invasive and cannot be applied to a wider patient population. Conventional modalities like ultrasound offer a qualitative assessment of fat and are more subjective. Non-enhanced CT scan has been effectively used for fat quantification based on Hounsfield values. MRI & more recently MRI PDFF (proton density fat fraction) offers accurate diagnosis, quantification, and monitoring of fatty liver disease in a noninvasive manner. This acts like an Imaging biomarker. Newer techniques like USG Elastography & MR Elastography help in the detection of fibrosis. Steatohepatitis and early liver fibrosis are reversible and it is crucial to detect and quantify to guide disease management. The radiologist can play a vital role in quantifying fat, detecting fibrosis, and early signs of chronic liver disease.

Keywords
- fatty liver
- steatohepatitis
- elastography

Introduction

Fatty liver refers to the accumulation of triglyceride within the hepatocytes which can lead to steatohepatitis. Subsequently, this can progress to liver cirrhosis and development of hepatocellular carcinoma (HCC). It manifests in two major forms which are alcoholic fatty liver disease caused by alcohol consumption and nonalcoholic fatty liver disease (NAFLD) which is related mainly to insulin resistance and metabolic syndrome. There has been rising evidence that NAFLD is associated with higher risk for cardiovascular disease and atherosclerosis and is an independent risk factor apart from other features of metabolic syndrome (►**Fig. 1**).[1] Fatty liver is a major global epidemic[2] with the reported prevalence of NAFLD in India ranging from 9 to 53%.[3] Given the huge population of India, fatty liver can cause heavy burden on the health care system and negatively impact the limited resources. In this review article, we will describe the pathophysiology of fatty liver, its effects on the liver, imaging features, and detection of fibrosis using elastography.

DOI https://doi.org/10.1055/s-0042-1742574.

Thieme Medical and Scientific Publishers Pvt. Ltd., A-12, 2nd Floor, Sector 2, Noida-201301 UP, India

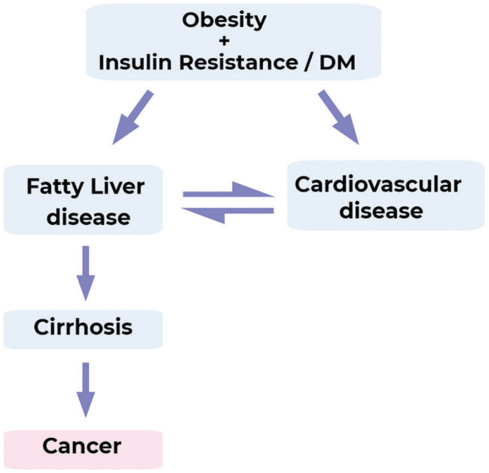

Fig. 1 Metabolic syndrome and association with fatty liver disease. DM, diabetes mellitus.

Pathophysiology of Non-alcoholic Fatty Liver Disease

NAFLD includes a broad spectrum of disorders ranging from simple hepatic steatosis to more severe steatohepatitis and cirrhosis (►**Fig. 2**). NAFLD has been rapidly recognized as a hepatic manifestation of metabolic syndrome.[4] The pathophysiology of NAFLD involves adipose tissue dysfunction and increased supply of free fatty acids to the liver, dysregulation of adipokines, excessive free fatty uptake by the liver, problems in hepatic lipid production and processing, and decreased lipid clearance by the liver.[5]

Increased free fatty acids in the blood have a role in the development of insulin resistance.[6] Insulin resistance leads to changes in lipid metabolism which includes increased peripheral lipolysis causing increased blood-free fatty acids, increased triglyceride synthesis, and increased hepatic uptake of the fatty acids which contribute to increased hepatocellular triglyceride accumulation.[7,8]

Apart from the supply of free fatty acids from the adipose tissues, the liver also performs de novo lipogenesis and produces triacylglycerols that are stored within the hepatocytes as lipid droplets. In normal healthy individuals, this de novo lipogenesis contributes to around 5% of triglyceride accumulation; however, in NAFLD, this share reaches upward up to 26%.[9] The triacylglycerol production in NAFLD is regulated by multiple factors like diet, hepatic insulin resistance, and genetics. The etiopathogenesis is demonstrated in the ►**Fig. 3**.

Progression of Nonalcoholic Fatty Liver Disease to Nonalcoholic Steatohepatitis and Cirrhosis

The metabolism of free fatty acid by oxidation in the liver results in the production of reactive oxygen species which are normally cleared by antioxidant pathways but get overwhelmed in nonalcoholic steatohepatitis (NASH) due to excessive uptake and production. The result is subsequent hepatocellular injury. There is recruitment of the hepatic stellate cells which are the resident fibroblastic cells of the liver and key players involved in the progression to fibrosis.[10] Due to chronic hepatic injury and inflammation, a wound healing process starts, and there is progressive deposition of extracellular matrix proteins which than later contribute to liver fibrosis (►**Fig. 4**).[11]

Pathologic Changes in Nonalcoholic Fatty Liver Disease and Nonalcoholic Steatohepatitis

The hepatocytes at the center of the lobule near the central vein (zone 3) are more prone to metabolic stress and accumulate fat faster than the periphery.[12] The pattern of fat deposition in the hepatocytes can be broadly classified into microvesicular and macrovesicular deposition (►**Fig. 5A** and **B**). In microvesicular deposition, there is small fatty cytoplasmic inclusions without any nuclear displacement. whereas, in macrovesicular deposition, the hepatocytes contain one large vacuole of fat which is larger than the nucleus and displaces it.[13] The macrovesicular pattern is the dominant finding in NAFLD and alcoholic fatty liver while a microvesicular pattern is seen in acute and recent liver injury such as acute fatty liver of pregnancy, Reye's syndrome, drug toxicities, and defect in β-oxidation of fatty acids.[14,15]

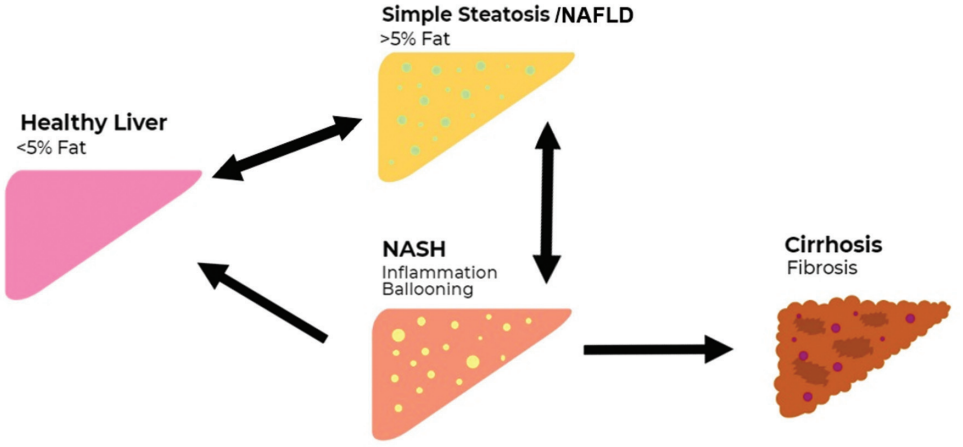

Fig. 2 Spectrum of fatty liver disease.. NAFLD and NASH are reversible. Cirrhosis is irreversible. NAFLD, nonalcoholic fatty liver disease; NASH, nonalcoholic steatohepatitis.

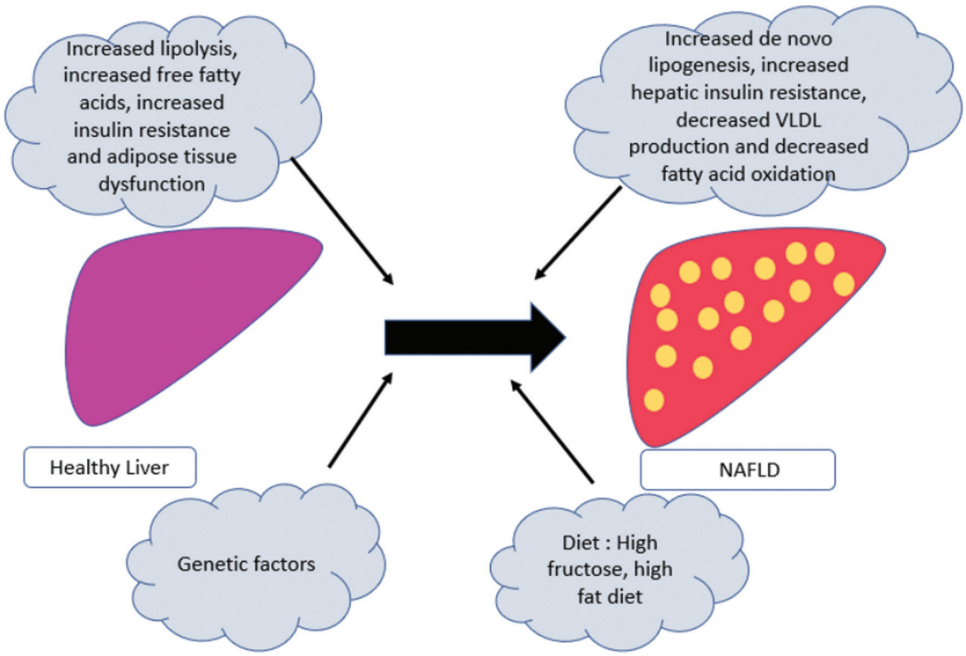

Fig. 3 Etiopathogenesis of nonalcoholic fatty liver disease (NAFLD).

The histological features are often seen in the NAFLD/NASH spectrum are steatosis, hepatocyte ballooning, lobular inflammation, and perisinusoidal fibrosis. The presence of fat alone or fat and inflammation without hepatocyte ballooning would qualify for NAFLD but not for NASH. Additional hepatocyte ballooning suggests NASH.[15] With progressive fibrosis, there is loss of normal architecture and formation of regenerating nodules which is a manifestation of liver cirrhosis (►**Fig. 5C-E**).

Detection and Quantification of Fat

Liver Biopsy

Liver biopsy is the gold standard in the diagnosis of fatty liver. In NASH, fat accumulation in the liver is often not uniform and a small hepatic tissue is sampled in biopsy which makes it suboptimal in its diagnosis.[16,17] Imaging modalities are noninvasive and play an important role in the diagnosis and monitoring of NAFLD and NASH.

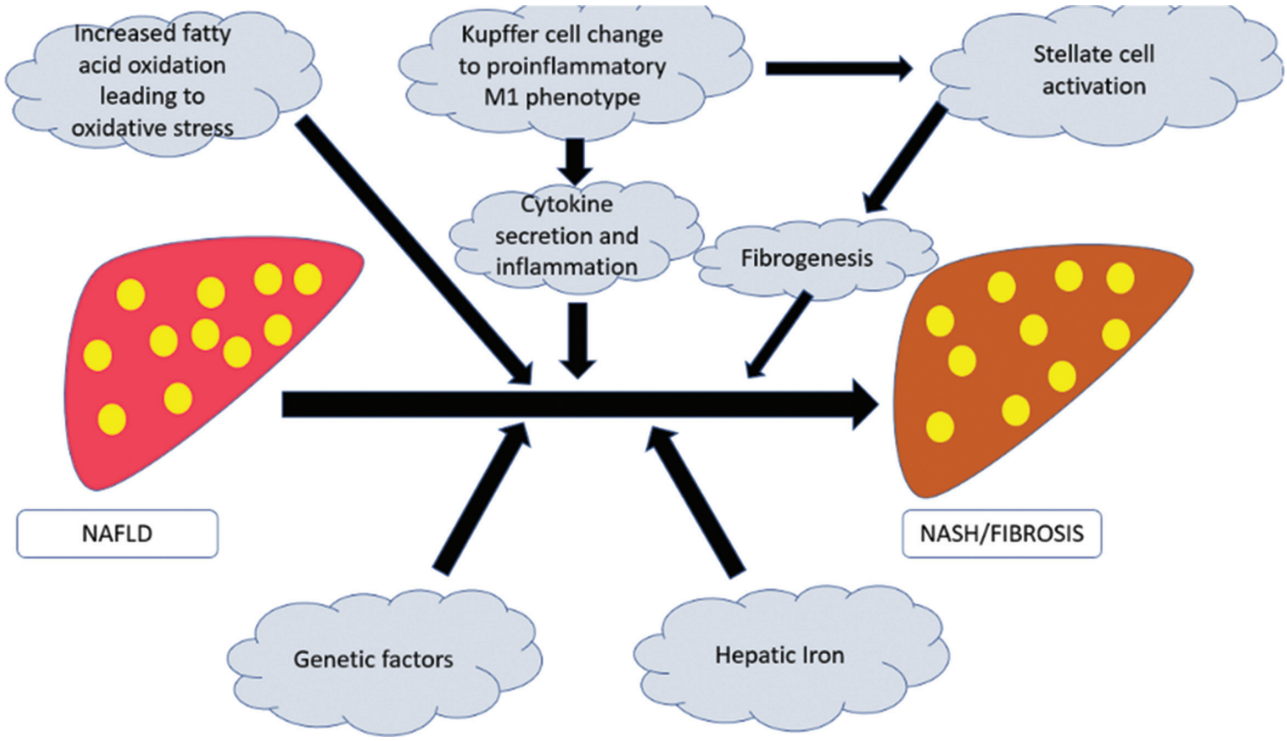

Fig. 4 Etiopathogenesis of nonalcoholic steatohepatitis (NASH).

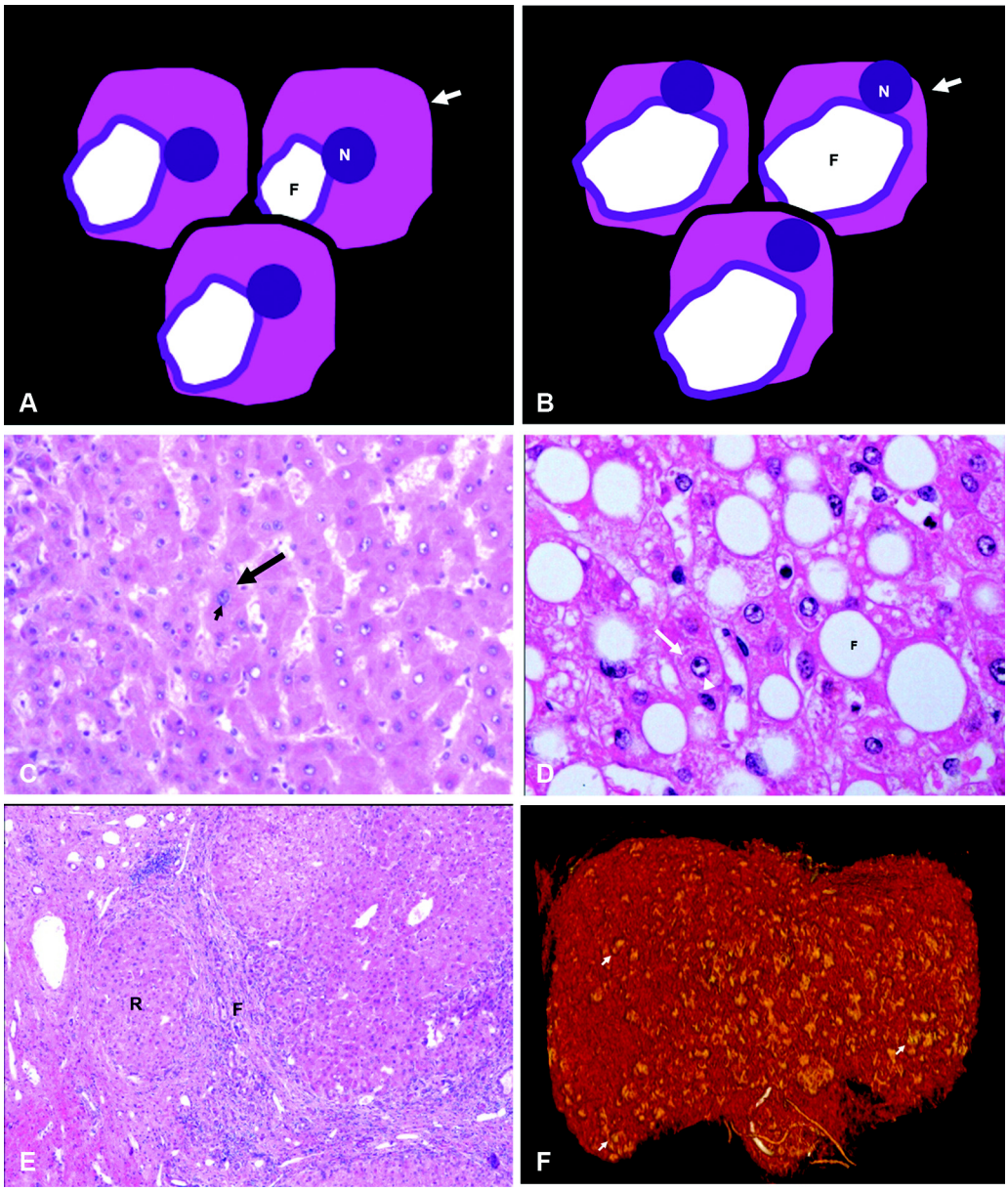

Fig. 5 Pathophysiology of NAFLD. (**A**) Microvesicular fat: schematic demonstrates small intracytoplasmic fat vacuoles (F) within the hepatocyte (white arrow) without displacing the nucleus (N). (**B**) Macrovesicular fat: schematic demonstrates large fat globule (F) within the hepatocyte (white arrow) displacing the nucleus (N). This gradually leads to cytoskeletal injury. (**C**) Histopathology of a normal liver demonstrates normal hepatocytes (long black arrow) in a hepatic lobule arranged in plates. Short black arrow is nucleus. (**D**) Histopathology in NAFLD, demonstrates fat globules accumulating in a hepatocyte (F). Long white arrow is a normal hepatocyte with nucleus (white arrowhead). (**E**) Histopathology in cirrhosis, demonstrates, that the internal architecture is distorted. R is regenerating nodule and F is fibrosis. (**F**) 3D Color VRT of a CECT demonstrates nodular liver surface with regenerating nodules (white small arrows). 3D, three-dimensional; CECT, contrast-enhanced computed tomography; NAFLD, nonalcoholic fatty liver disease. (Image Courtesy [C, D and E]: Department of Pathology, Kokilaben Hospital, Mumbai).

Ultrasound

Conventional Ultrasound

Conventional ultrasound is the initial modality for screening of fatty liver, as it is widely available, cheap, radiation free, and portable.[18,19] On conventional B-mode ultrasound, echotexture of normal liver is equal to or slightly higher than spleen and renal cortex (►**Fig. 6A**). When fat globules accumulate in hepatocytes, it causes back scatter of ultrasound beams resulting in more sound waves reaching the transducer which is seen as raised echotexture of liver (►**Fig. 6B**). These intracellular fat globules also prevent ultrasound beam reaching deeper tissues which cause blurring or poor visibility of deeper structures like intrahepatic portal veins, hepatic veins, diaphragm, and others (►**Fig. 6C**).[20]

Fatty liver can be graded as mild, moderate, and severe. In mild fatty liver, there is only raised echotexture of liver, whereas in moderate fatty liver, there is blurring of echogenic walls of intrahepatic portal and hepatic veins in addition to raised echotexture; however, the diaphragm is visible distinctly. In a severe fatty liver, the dome of the diaphragm is not visible separately.

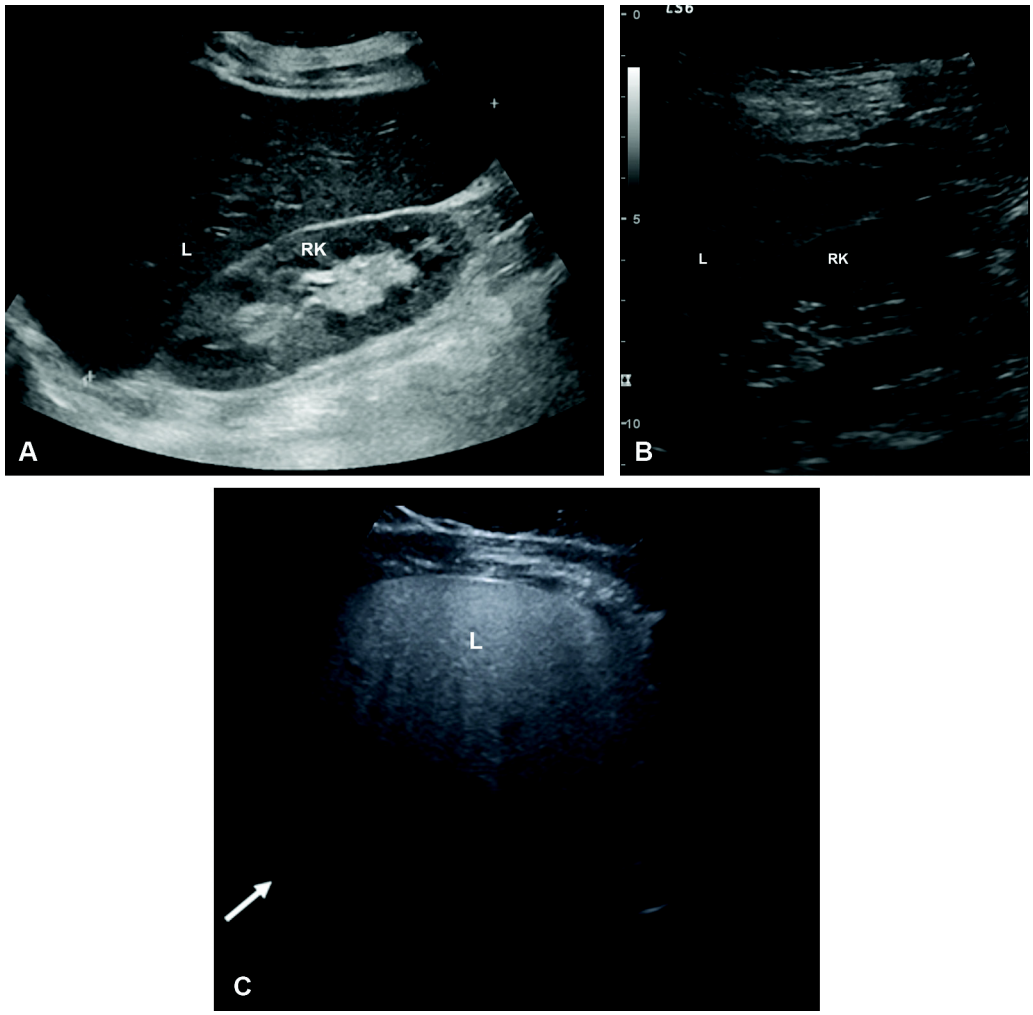

Fig. 6 Fatty liver appearance on ultrasound. (**A**) 2D ultrasound demonstrates normal echogenicity of the liver (L), similar to the renal cortex (RK). (**B**): 2D ultrasound demonstrates liver (L) with increased echogenicity compared with the right kidney (RK). This is suggestive of moderate fatty accumulation. (**C**) 2D ultrasound demonstrates enlarged liver (L) with significantly raised echogenicity. The diaphragm is poorly visualized (white arrow). 2D, two-dimensional.

Conventional ultrasound is useful for qualitative assessment and being subjective investigation, it is prone for interobserver variability.[21,22] More so, assessment of liver echotexture is technically difficult in obese patients.[12,21] However, iron in the hepatic parenchyma has negligible effect on ultrasound beam as opposed to computed tomography (CT) scan and magnetic resonance imaging (MRI) as described in the subsequent sections.[23,24]

Newer ultrasound techniques which can be helpful in quantitative assessment like speed of sound, attenuation coefficient, controlled attenuation parameter, and backscatter coefficient are still being investigated for its usefulness.

There is a long latent period to develop hepatic fibrosis from simple steatosis. Neither conventional nor quantitative ultrasound techniques can differentiate simple hepatic steatosis from steatohepatitis or hepatic fibrosis.

Computed Tomography

CT uses attenuation of liver parenchyma as a parameter to quantify fatty in the liver using Hounsfield's Units (HU). In hepatic steatosis, attenuation value of liver declines with the increase in degree of fat accumulation.[23,24] On plain CT, attenuation value of normal liver is 50 to 65 HU (8–10 HU more than spleen).[18] Hepatic steatosis can be predicted when absolute CT attenuation value of liver is less than 40 or 10 HU less than spleen[25–30] (►**Fig. 7A**).

Liver attenuation index (LAI) is another method of predicting hepatic steatosis. Multiple measurements are taken, typically 25 from the liver and 9 from spleen. Thereafter, mean HU of the liver and mean HU of the spleen is calculated. Park et al calculated LAI by hepatic-to-splenic attenuation ratio. They showed that if the ratio is less than 0.8, it is highly specific for moderate-to-severe (>30%) fatty liver.[31] Another study by Limanond et al calculated hepatic attenuation index by hepatosplenic attenuation difference. They demonstrated that, if the difference is more than 5 HU, it indicates nonsignificant fat content (0–5%), difference of −10 to 5 HU indicates mild-to-moderate fat content (6–30%) and when difference is less than −10 HU, it indicates severe fat content (>30%).[27] However, the liver attenuation can be affected by

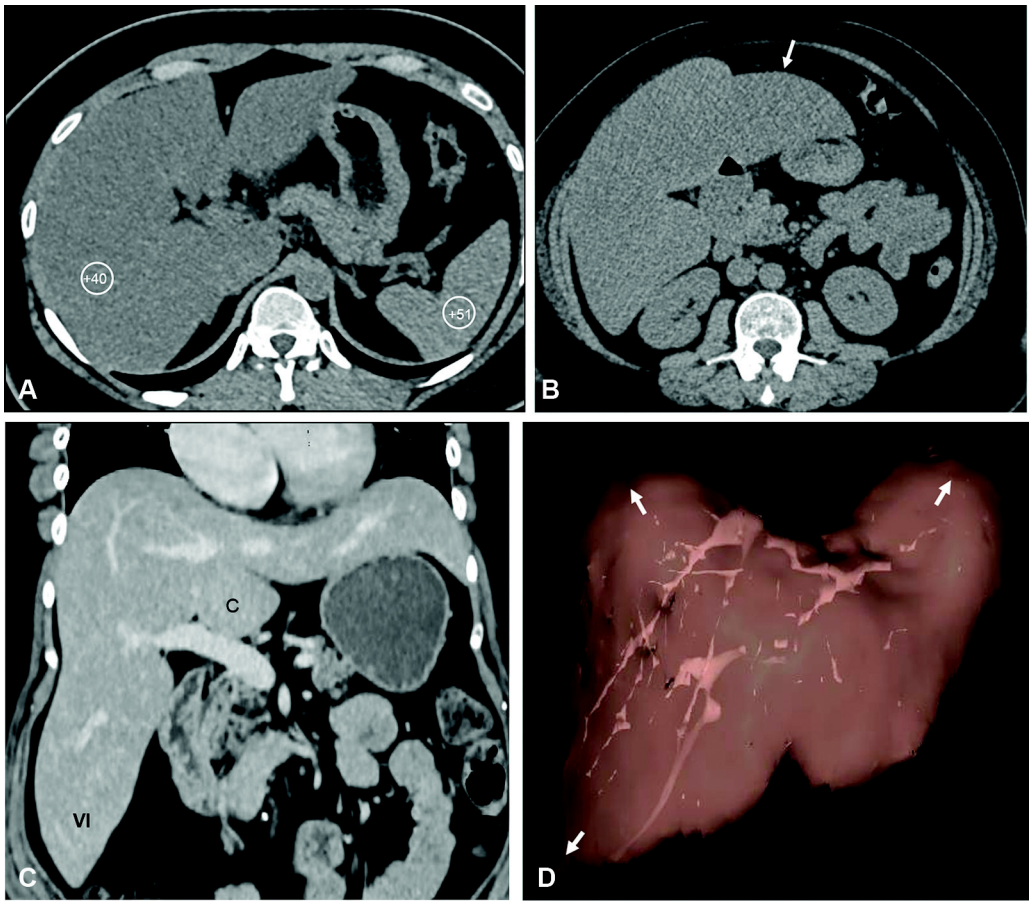

Fig. 7 Fatty liver appearance on CT scan. Image. (**A**) NECT demonstrates HU value of the liver lower than spleen. This is suggestive of fatty accumulation in the liver. Note normal lobar anatomy and smooth margins. (**B**) NECT of a different patient, demonstrates enlargement with altered lobar anatomy. The margins are bulging without any surface nodularity (white arrow). This is suggestive of a long-standing fatty accumulation. (**C**) CECT in coronal plane demonstrates enlarged liver with altered lobar anatomy. C is the caudate lobe and VI is the liver segment. (**D**) CECT, 3D surface volume rendering of the same patient as ►**Fig. 3C**. Enlargement happening in all directions (white small arrow). 3D, three-dimensional; CECT, contrast-enhanced computed tomography; HU, Hounsfield's unit; NECT, non-enhanced CT.

intrahepatic iron, glycogen deposition, hepatic injury secondary to hepatitis, drugs, radiation, etc., which can be a confounding factor.[27,32] ►**Table 1** describes various values for significant fat in the liver.

In NAFLD, there is gradual and generalized hepatic enlargement causing increase in hepatic dimension/span in midclavicular line, enlargement of the caudate lobe, and extension of the left lateral segment toward the spleen (►**Fig. 7B-D**). As the hepatic steatosis progresses to fibrosis, the margins become nodular and eventually liver loses fat and will shrink in size with typical features of cirrhosis, indistinguishable from other etiology. Three-dimensional (3D) volume rendering technique (VRT) surface rendering can easily demonstrate the gross appearance of the liver and can distinguish normal liver from precirrhotic liver fibrosis which may not be so apparent on the two-dimensional (2D) images (►**Fig. 8**).

Table 1 Hounsfield's unit (HU) based fat quantification on CT

	Significant fat in liver
1.	<40 HU at 120 kVp
2.	Liver attenuation index (LAI): < -10
3.	Liver spleen attenuation ratio: <0.8

Abbreviations: CT, computed tomography; LAI, liver attenuation index.

Contrast-Enhanced Computed Tomography

Difference of liver to spleen attenuation of at least 20 HU in portal venous phase (when scan performed 80 to 100s after injecting the intravenous contrast) may indicate hepatic steatosis.[33] However, this is unreliable as it depends on the rate of contrast injection, time of acquisition, and site of injection.[34]

Dual-Energy Computed Tomography Scan

Using attenuation difference of tissue at two different energy levels performed at 80 and 140 kVp and material decomposition technique dual-energy CT (DECT) can produce iodine, water, and fat-weighted images, and also enables to quantify fat content.[35]

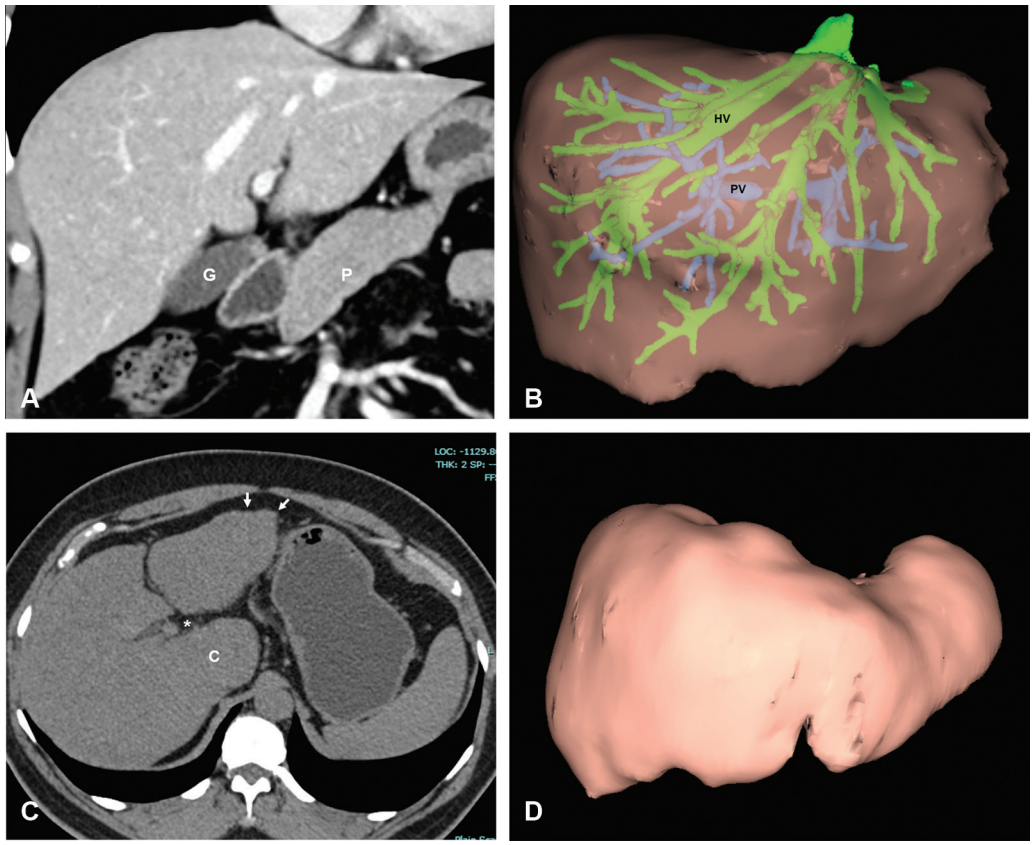

Fig. 8 Liver rendering in a normal liver vs NAFLD related cirrhosis. (**A**) CECT 3D surface volume rendering of a normal liver. HV is hepatic vein (green color) and PV is portal vein (blue color). (**B**) NECT demonstrates liver has altered lobar anatomy and diffuse fatty accumulation. The caudate lobe is enlarged *C). The liver margins in the left lobe show subtle nodularity (small white arrow). There is prominence of fissures. Findings are suggestive of liver cirrhosis, (**C**) CECT 3D surface volume rendering of the liver in the same patient as (**B**). This liver surface has nodular margins and altered lobar anatomy. 3D, three-dimensional; CECT, contrast-enhanced computed tomography; NAFLD, nonalcoholic fatty liver disease.

Computed Tomography Fibrosis Score

It aids in diagnosis of precirrhotic hepatic fibrosis. It is calculated by division of sum of liver vein diameters by the caudate-to-right-lobe ratio.[36] CT fibrosis score less than 24 indicates precirrhotic hepatic fibrosis (sensitivity of 83% and specificity of 76%) and score less than 20 indicates hepatic cirrhosis (sensitivity of 88% and a specificity of 82%).[36]

Magnetic Resonance Imaging Fat Quantification

The water and fat molecules have unique chemical structures which lead to their different magnetic properties.

Water is a small rapidly rotating molecule with an electronegative oxygen atom that generates polarity exposing them to the full external magnetic field force. So, they resonate faster than other hydrogen atoms and have longer T1 and T2 relaxation times.

Fat is a slowly moving large molecule with an electroneutral long carbon chain with an electron cloud that provides shielding from external magnetic fields. Thus, fat has shorter T1 and T2 relaxation times.

Fatty accumulation in the liver shows increased signal intensity of the liver on T1- and T2-weighted spin-echo images. Various methods have been developed for hepatic fat estimation to suppress, increase, or separate water and fat signals by exploiting differences in T1, resonant frequency, or both. Commonly, liver fat estimation is done in the form of fat fraction (FF) which is generated in two ways. One is signal FF (liver signal attributable to fat) and the other is proton density FF (PDFF; the fraction of mobile protons in liver attributable to fat; ►**Fig. 9**).

Signal Fat Fraction Estimation

Chemical Fat Suppression (T1-Weighted Fat-Suppressed Image)

Magnitude images are compared in two sets of images with and without fat suppression. The fat suppression is achieved either with a radiofrequency (RF)-pulse tuned to the fat resonance frequency together with a spoiler gradient saturates and dephases fat protons or selective water excitation. So that only water produces a signal to achieve fat suppression.

In the presence of macroscopic fat, the signal is higher on the nonfat-suppressed images than on the fat-suppressed images. The difference in signal intensity between nonfat-suppressed and fat-suppressed images is assumed to represent the fat signal (F) and calculate FF.

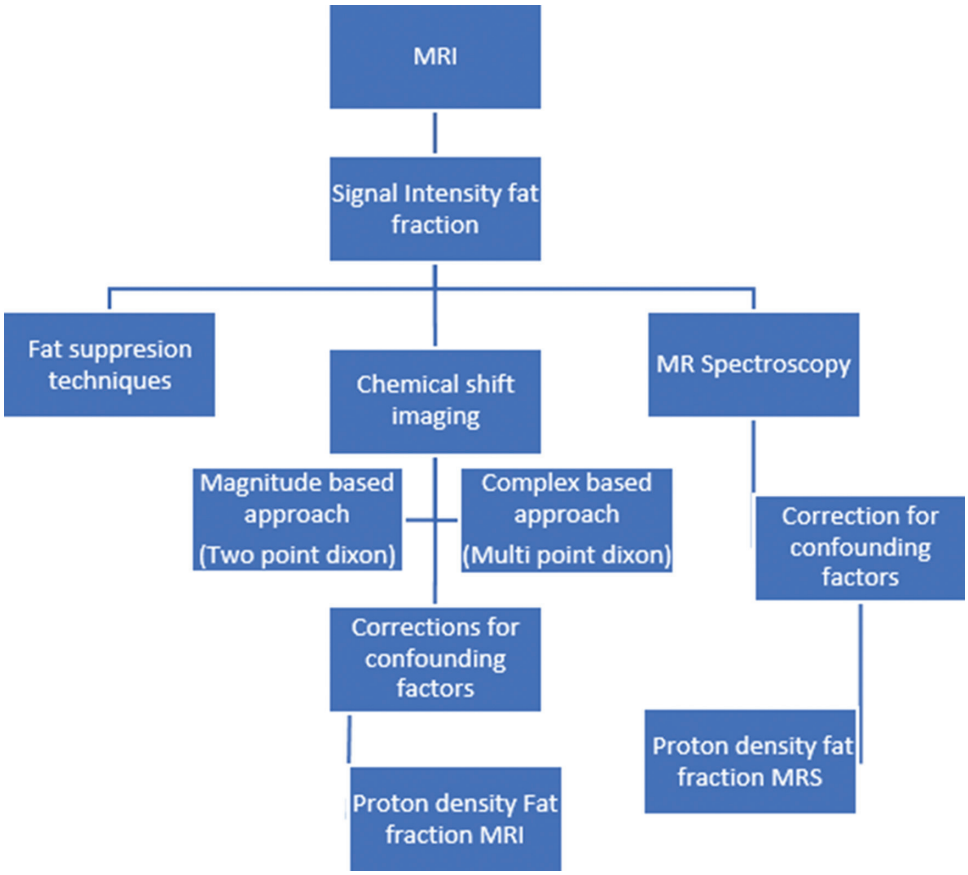

Fig. 9 Technique for MR fat quantification. MR, magnetic resonance; MRI, MR imaging; MRS, MR spectroscopy.

This method estimates the signal FF with a dynamic range of 0 to 100%.

Due to the inhomogeneous main magnetic field (Bo), there is incomplete fat suppression or even unintentional water suppression throughout the liver.[37]

Chemical Shift Imaging (In- and Out-Phase Imaging)

Water and fat protons have different resonance frequencies (water peak [4.7 parts per million (ppm)] and the dominant fat peak [1.3 ppm]). The difference in this resonance frequency is known as the water–fat chemical shift which is approximately 3.5 ppm. It increases with increasing magnetic field strength. It can be calculated by the Larmor frequency under specific field's strength multiplied by 3.5.

In a 1.5-T scanner with a Larmor's frequency of 64 MHz, the fat–water frequency difference will be around $\Delta f \approx 220$ Hz. At a 3.0-T scanner with a Larmor's frequency of 128 MHz, the fat–water frequency difference will be around 440 Hz.

Their spins go in and opposed-phase with each other as a function of time. The period of this cycling is $1/\Delta f$, where Δf is the frequency offset between the spins. Thus at 1.5 T, the phase cycling period is 1/220 Hz or approximately 4.6 ms.

On a 1.5-T scanner, signals from fat and water are in phase every 4.6 ms, out of phase at 2.3 ms, and their multiples. At 3 T, the signals are in phase at 2.3 ms and out of phase at 1.15 ms and their multiples thereafter (half of the 1.5 T values; ►**Fig. 10**).

Chemical shift imaging method uses this concept. After single excitation, two sets of spin-echo images are acquired with different echo times, the first with fat and water signals in-phase and the second with the fat and water signals are opposed phase. Chemical shift MRI is the investigation of choice in cases with focal nodular or multifocal fat deposition/sparing that may be confused with liver metastases on ultrasound or CT (►**Fig. 11**).

Two main chemical shift-based approaches are magnitude based (2-point Dixon) and complex-based (multipoint Dixon).

Magnitude-Based Chemical Shift (2-Point Dixon)

Dixon suggested that the in-phase and out-of-phase images can be combined, so that fat-only and water-only images can be generated. Thus, the water-only image becomes fat suppressed.[38,39]

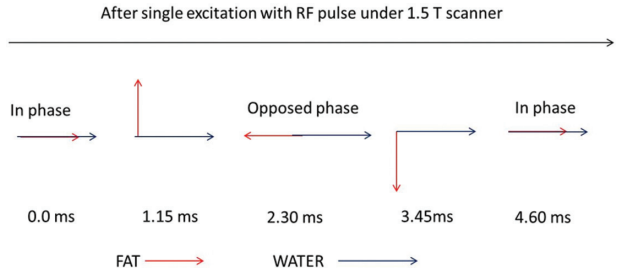

Fig. 10 Concept of chemical shift imaging. RF, radiofrequency.

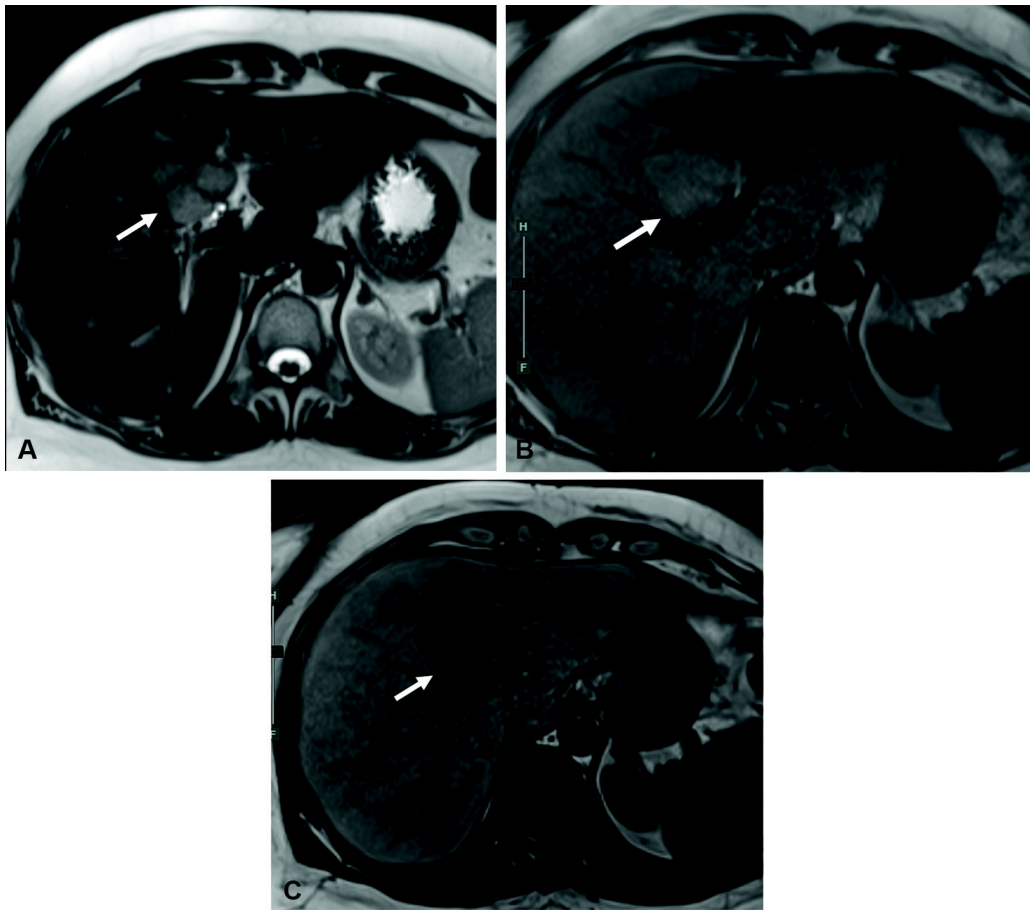

Fig. 11 Magnitude based chemical shift imaging—IOP imaging. (**A**) T2-weighted HASTE axial image demonstrates focal intermediate to hyperintense lesion in segment 4 (white arrow), (**B**) T1-weighted In-phase axial image at the same level demonstrates corresponding hyperintense lesion (white arrow). (**C**) T1-weighted Out-phase axial image at the same level demonstrates significant drop in the signal (white arrow). HASTE, half fourier single shot turbo spin echo; IOP, in and out phase imaging.

This phenomenon is used clinically to identify and quantify the fat content in the liver. This is often called "dual-phase" or "dual-echo" or "2-point Dixon" imaging. Lesions whose signal intensities drop significantly on the opposed phase images are likely to contain microscopic fat which is intracellular fat. This intracellular fat can be micro- or macrovesicular. The opposed phase cancellation effect produces misregistration between fat and water leading to a specific type of MR artifact, called the "India ink artifact" or "chemical shift artifact" seen along with the interface of water containing abdominal structures like liver and spleen surrounded by fat (►**Fig. 12**).

Liver signal FF is calculated with the following formula:

$FF = IN\text{-}OPP / 2 \times IN$

$IN = W + F$

$OPP = W - F$

$(IN + OPP) / 2 = [(W + F) + (W - F)] / 2 = (2W) / 2 = W \rightarrow$ water-only image

$(IN - OPP) / 2 = [(W + F) - (W - F)] / 2 = (2F) / 2 = F \rightarrow$ fat-only image

(IN: signal intensity from the in-phase image, OPP, signal intensity from the opposed-phase image, W and F are the signal contributions from water and fat, and the signal intensity from fat is less than the signal intensity from water).

This formula can be applied to a region of interest or voxel basis to create a signal FF map. It is used only if both in-phase and opposed phase are derived after the same excitation.

This technique does not accurately reflect the concentration of fat within the liver. The only dynamic range of 0 to 50% signal FF can be calculated because, in magnitude imaging, a single pair of opposed-phase and in-phase echoes cannot distinguish between water- and fat-dominant tissues. For example, a tissue with 20% fat by signal composition would appear to have the same signal FF as a tissue with 80% fat, both tissues would be assigned a signal FF of 20%. FFs greater than 50% are uncommon in the liver.[40,41]

Complex Chemical Shift-Based Water and Fat Separation (Multipoint Dixon)

The complex chemical shift utilizes both magnitude and phase information from three or more images acquired at echo times appropriate for the separation of water and fat signals.[42]

The complex-based approach allows full separation of water and fat signals to achieve a dynamic range of 0 to 100% signal FF which offers fat quantification, regardless of the tissue type (liver, adipose, bone marrow, etc.).[43]

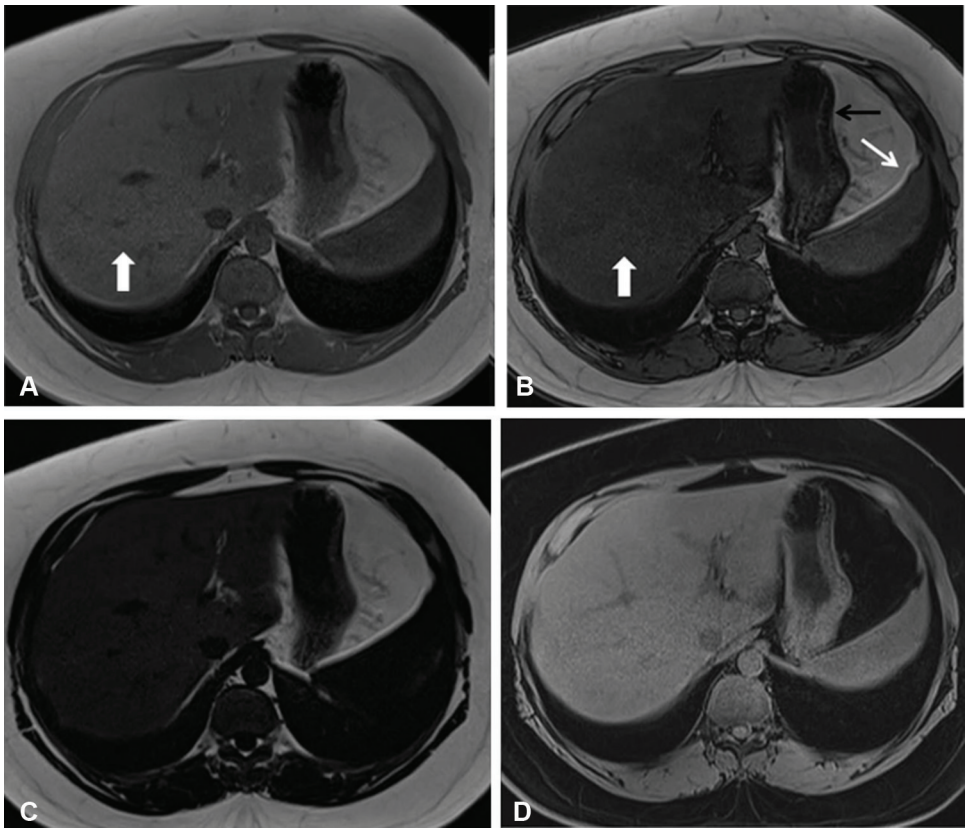

Fig. 12 Magnitude base chemical shift imaging–2-point Dixon. Demonstration of T1-weighted GRE (2-point Dixon), which gives four series of images: (**A**) in phase, (**B**) opposed phase, –(**C**) fat only, and (**D**) water only. There is a drop in the signal intensity in the opposed phase image compared with in phase (solid white arrow) to suggest diffuse fatty infiltration. Also note, chemical shift artifact is bright (thin white arrow) and dark bands (thin black arrow) along margins of liver and spleen which is also helpful in identification of opposed phase sequence (**B**).

The signal FF map may not accurately reflect the concentration of fat within the liver due to many confounding factors. Techniques that correct all confounding factors measure proton density FF.[44–47]

Confounding Factors

If all confounders are corrected, the calculated FF becomes the proton-density FF (PDFF). The necessary corrections can be applied to magnitude and complex based chemical shift or combination of both (hybrid) to obtain MRI PDFF (►**Table 2**).[48]

Magnetic Resonance Imaging Proton Density Fat Fraction

Typically, a 3D multiecho gradient (six echoes) VIBE (Volumetric Interpolated Breath Hold Examinaton). Sequence with Dixon reconstructions and correction for $T2^*$ in the presence of iron is used. It requires a single similar breath-hold of 18 to 20 seconds like e–Dixon. It provides seven image series: water, fat, FF, WF (water fraction), effective $R2^*$map, effective $T2^*$ map, and goodness-of-fit map for quality control (►**Fig. 13**).

$R2^*$ is the inverse of $T2^*$. Thus, A higher $R2^*$ and lower $T2^*$ both correlate with higher iron content. $R2^*$ values are corrected for fat content and FF is corrected for $T2^*$ effects. $R2^*$ value is converted to liver iron concentration micromole Fe/g or mg Fe/g by a conversion factor of a specific device. Normal value is 36 micromole Fe/g or 2 mg Fe/g. For simplification we can use LIC (μmol) = $R2^*/3.2$.[49]

Final results show color bars of the two biomarkers: PDFF and $R2^*$ ($1/T2^*$), both as average values calculated over segmented liver volume and region of interest (ROI; ►**Fig. 14**). During postprocessing, PDFF, and $R2^*$ can also be measured by placing the ROI in the useful hepatic segments in the FF and effective $R2^*$ series. It is suggested to draw a large ROI covering a single lobe of the liver or hepatic segment avoiding gall bladder and vessels rather than drawing multiple ROIs within the liver to measure accurate PDFF.[50]

Role of Magnetic Resonance Imaging Proton Density Fat Fraction in Nonalcoholic Steatohepatitis

PDFF is noninvasive MRI biomarker to accurately quantify FF in the liver and is used as an endpoint in NASH trials.[51]

Earlier the liver biopsy was considered the endpoint of NASH trials. But, the biopsy is invasive and provides a small specimen assessment. MRI PDFF provides larger coverage with the noninvasive accurate alternative.

There is a positive correlation of MRI PDFF with liver biopsy and ex vivo human liver specimens to assess hepatic steatosis from absent fat to severe fatty deposition. However, this correlation drops with the development of fibrosis.[52–54]

Permutt et al demonstrated that average MRI-determined PDFF and histology-determined steatosis grade remained relatively stable at fibrosis stages 0 to 3 but dropped significantly at stage 4.[55]

Table 2 Confounding factors in the MRI fat quantification using chemical shift imaging

Confounding factor	Affected techniques	Description	Correction	Drawbacks
T1 bias	T1-weighted imaging techniques are affected	Amplification of fat signal due to short T1	Long TR or low flip angle for chemical shift-based MRI[71,72]	Long TR values lengthen the acquisition and breath-hold time. Very low flip angles lead to reduce SNR
T2 bias	MRS (utilize refocusing pulses to generate echoes)	Amplification of fat signal due to short T2 relaxation of water	Use the shortest possible TE or collect spectra at multiple TEs	
T2 * effect	Chemical shift-based MRI	T2* decay leads to increasing signal loss with increasing TE which is amplified by the presence of iron	Inclusion of T2* into the signal model or separate acquisition of T2*	T2* correction leads to reduction in SNR which is improved by increasing the number of echoes in the echo train, which provides a better sampling of the signal decay. At least 6 echoes are needed for accurate separation of water and fat with T2* correction[73]
Spectral complexity of fat		The two peaks (5.3 and 4.2 ppm) that lie close to the water resonance and cannot be differentiated from the water peak and would be incorrectly mapped to water signal	Information in the four visible peaks can derive triglyceride chemical structure to determine the type and calculation of the full fat spectrum[74]	
Noise bias	Chemical shift-based MRI	Areas of low-fat signal have only positive noise after the magnitude operation[71]	Magnitude discrimination and phase constrained reconstruction	
Eddy currents	Complex-based chemical shift MRI	Rapid switching of gradients during image acquisition leads to unpredicted phase shifts on images acquired at different echo times	Magnitude based methods or hybrid techniques	
J coupling	MRS and spin-echo sequences	J coupling increases with increased TE	STEAM (shorter TE) is preferred with a shorter range to avoid T2 bias	
Field strength		T1, T2*, and chemical shift effect have a linear relationship with field strength	Correction of T1 bias and T2* effect with spectral complexity	

Abbreviations: MR, magnetic resonance; MRI, MR imaging; MRS, MR spectroscopy; SNR, signal-to-noise ratio; STEAM, stimulated echo acquisition mode; TE, time to echo; TR, repetition time.

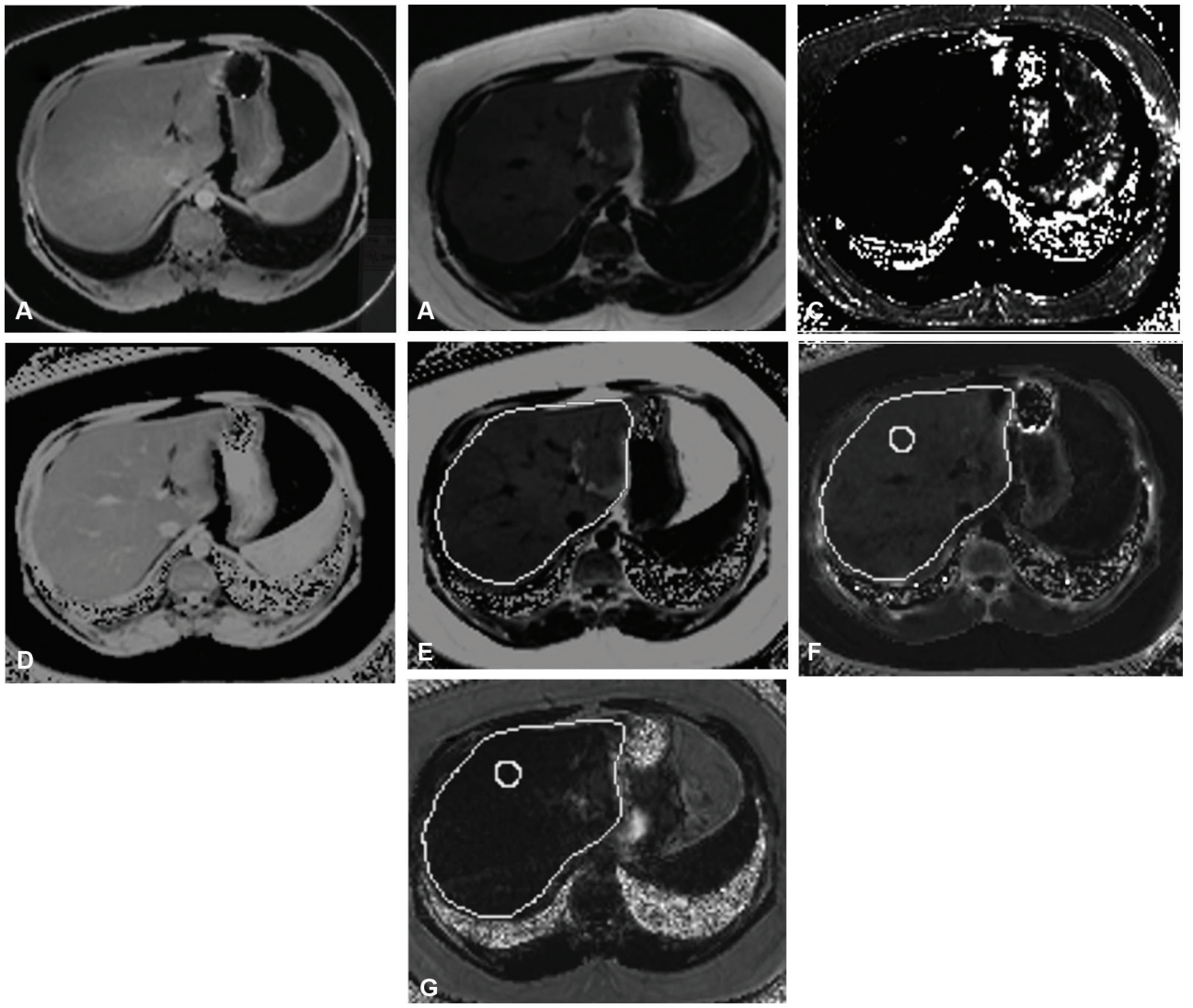

Fig. 13 Complex based approach proton density fat fraction—6-point Dixon. Set of seven images obtained from the sequence: (**A**) water only image, (**B**) fat only image, (**C**) effectiveT2* map, (**D**) water fraction, (**E**) fat fraction, (**F**) effective R2 * map, and (**G**) goodness of fit map. ROI can be made on the "fat fraction" image and fat percentage can be obtained. ROI, region of interest.

Standardized NASH histologic scoring system for NAFLD is according to the proportion of hepatocytes that contained microvesicles of fat by using the following ordinal scale: grade 0 for less than 5%, grade 1 for 5 to 33%, grade 2 for 33 to 66%, and grade 3 for more than 66%.[56]

Hepatic steatosis grading by MRI PDFF is histopathologically validated and incorporated in the NASH clinical trials by following PDFF threshold cut-off:

Between grades 0 and 1 = 6.4%, between grades 1 and 2 = 17.4%, and between grades 2 and 3 = 22.1%.[57,58] These grading systems were further validated by various studies.[59] Thus, MRI PDFF is considered superior to liver biopsy and acts as a surrogate biomarker along with MR elastography (MRE)for NASH clinical trials.[60]

There is high intra- and interexamination repeatability and agreement for MRI-based PDFF in obese children and adults.[61] Negrete et al demonstrated that MRI-based PDFF assessments showed excellent interexamination precision for each hepatic segment, each hepatic lobe and the whole liver.[62] MRI PDFF is reproducible with different field strengths (like 1.5 and 3 T) with excellent agreements.[63–65]

An analysis by Noureddin et al further demonstrated that patients who had an increase or decrease in MRI-PDFF of $\geq$1% showed a parallel increase or decrease in their body weight and serum alanine and aspartate aminotransferases at week 24 ($p < 0.05$), and this small increase or decrease in hepatic steatosis could not be detected with liver biopsy–based histology assessments.[66]

There are various longitudinal studies that have assessed MRI PDFF for the response of the fat content to various medications with biopsy confirmation in support of NASH trials.[67–71]

In clinical practice, Doycheva et al assessed the feasibility of screening for NAFLD with MRI-PDFF in the primary care setting and determined that the prevalence of NAFLD among type-2 diabetics was 65%.[72]

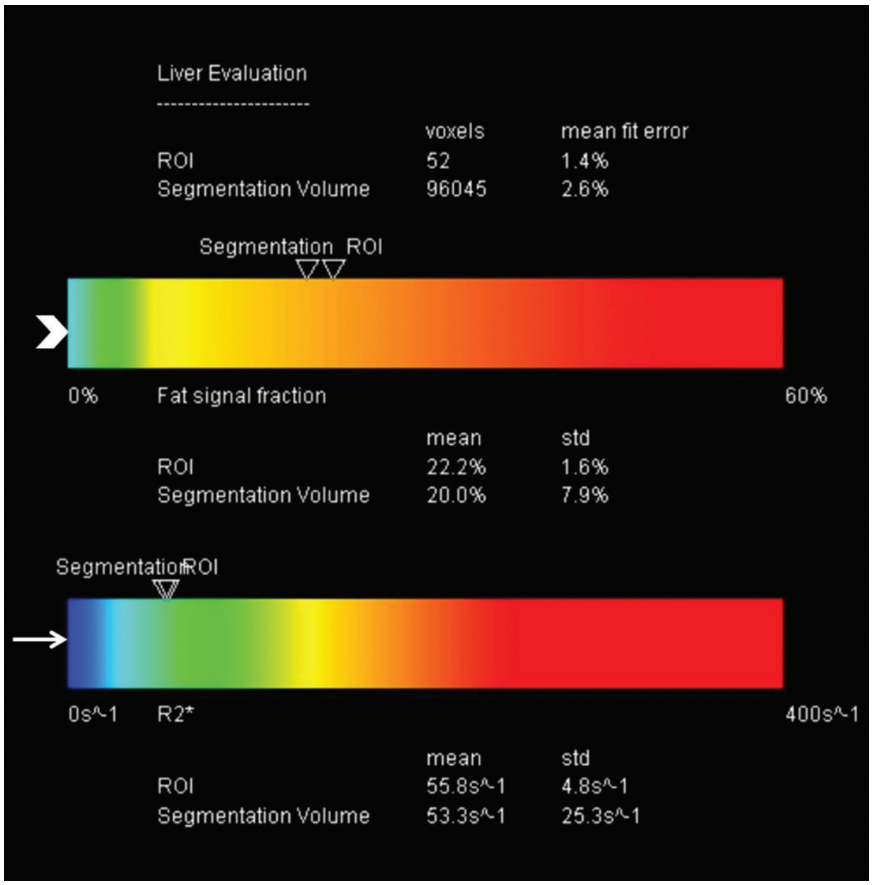

Fig. 14 Protein density fat fraction—color map. Same patient as in ►**Fig. 7**. Top color bar (arrowhead) shows 22% fat fraction suggestive of grade-2 fatty infiltration by ROI method. On segmentation of the entire level, the accuracy is reduced and the fat quantification is 20%. Bottom color bar (white arrow) shows the Iron quantification, which is R2 * vale of 55.8/s and is within normal limits. ROI, region of interest.

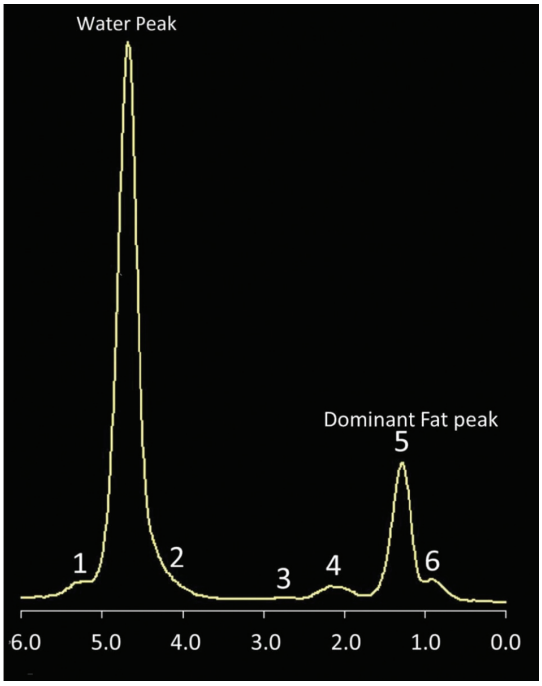

Fig. 15 MR spectroscopy—fat and water peaks. Liver spectrum from a healthy demonstrates presence of multiple fat peaks (1 to 6 no's). X axis shows relative resonance frequency in ppm. Two out of the six fat peaks are buried under water peak at 4.7 ppm. Dominant fat peak is at 1.3 p.m. MR, magnetic resonance.

Magnetic Resonance Spectroscopy

MR spectroscopy (MRS) is a direct method to separate fat and water components and measures signal FF.

The water spectrum consists of a single resonance peak (4.7 ppm). Because, the two hydrogen protons have the same chemical environment, experience similar magnetic fields, and resonate at the same frequency in the water molecule. On the other side, the fat proton spectrum is complex, as the multiple hydrogen protons in fat have different chemical environments, experience nonidentical magnetic fields, and resonate at different frequencies.

The liver fat protons produce nine resonant frequencies ex vivo at high field strength. In vivo, at clinical field strengths, there are six resolvable distinct fat peaks (5.3, 4.2, 2.7, 2.1, 1.3, and 0.9 ppm) including one dominant peak (1.3 ppm; ►**Fig. 15**). However, two peaks (5.3 and 4.2 ppm) cannot be clearly distinguished from water. The liver spectrum or preexisting spectral modeling can be used to rectify fat peaks included in water in MRS. The area under each visible peak is quantified. The fat signal then is calculated as the sum of these areas of the fat peaks (2.1, 1.3, and 0.9 ppm) or as the area of the dominant CH2 peak (1.3 ppm). The signal FF can then be given as the fat signal divided by the sum of the water and fat peaks areas. The signal FF with MRS has a dynamic range of 0 to 100%.[73]

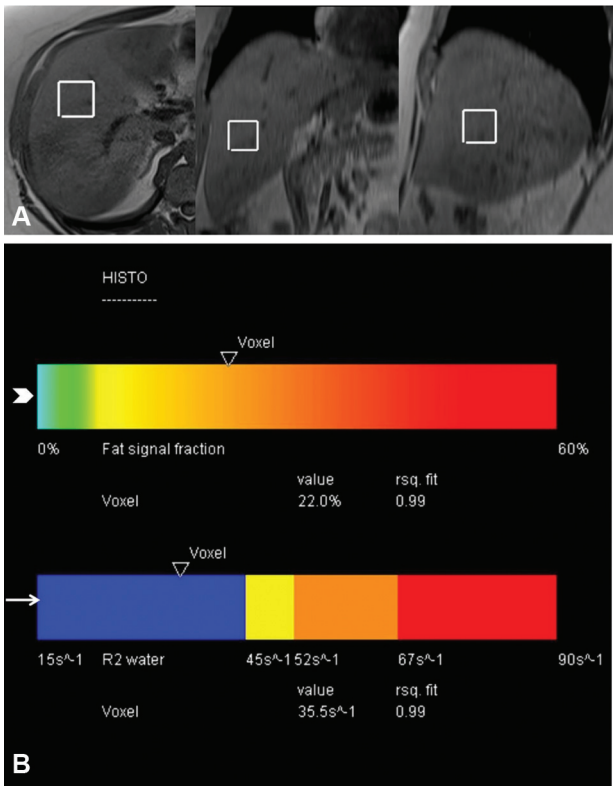

Fig. 16 MR Spectroscopy—protein density fat fraction. (**A**) demonstrates three localizer sequences to define the location of the voxel ($3 \times 3 \times 3\ cm^3$) avoiding gallbladder and vessels. (**B**) Demonstrates two color bars with fat fraction in the top (white arrow head) and R2 water signal bar below (white arrow) which shows 22% fat content suggestive of fatty infiltration. Iron content (R2 water) is within normal limits. MR, magnetic resonance.

Technique for MRS: typically, STEAM technique is used for MRS. This is a multiecho shorter TE (12 ms) sequence acquired in a single voxel. A single voxel ($2 \times 2 \times 2$ or $3 \times 3 \times 3\ cm^3$) is manually placed in the liver parenchyma, using localizer images avoiding liver edges, large vessels, and large bile ducts (►**Fig. 16A**). Shimming is performed to achieve a homogeneous magnetic field across the voxel. No water or fat saturation should be employed. Spatial saturation bands are not used because saturation bands may partially saturate the signals arising from the voxel, leading to errors in the proportion of the liver signal attributed to fat. There is preference to collect spectra during a single breath hold, approximately 15 seconds. Necessary confounder factors corrections can be applied to MRS to obtain MRS PDFF. The sequence contains an algorithm to get FF and water R2 (not R2 * since this is a spin-echo sequence) which are represented in color bars (►**Fig. 16B**).

MRS PDFF is considered the most accurate method but it allows limited voxel evaluation and requires technical expertise and analysis.[74] It is difficult to replicate voxel placement leading to sampling variability. However, it serves as the reference standard for MRI PDFF.[75]

Role of Contrast Magnetic Resonance Imaging

Contrast-enhanced MRI (CEMRI) using gadoxetic acid has been shown to have potential in differentiating simple steatosis from NASH. The mean liver enhancement is found to be lower in NASH compared with simple steatosis likely due to increased hepatocyte volume reducing the sinusoidal space leading to the contrast uptake.[76] Poor hepatic uptake of USPIO has been seen in patients NASH than in simple steatosis.[77]

Elastography

Liver fibrosis is a dynamic and a heterogeneous process. It gradually happens over a long time. There is a big window before cirrhosis is set in. During this window, if fibrosis is detected in early stages, it can be reversed by medical therapy. Liver biopsy is the gold standard; however, it is invasive and the sample is very small. It is not representative of the entire liver, especially as this process is not homogenous.[78] Elastography is a novel technique which uses property of tissue stiffness/elasticity and detect fibrosis noninvasively. The basic principle of the technique is stress (force per unit area) is applied to the tissue and analyze the strain (expansion per unit area) induced in tissue.[33,79] Depending on the technique of applying stress to the tissue elastography broadly classified in strain imaging and shear wave imaging.[80]

Strain imaging uses static (stress induced by manual compression) and quasistatic (stress induced by physiological vibrations inside the body) techniques and produce qualitative color map and strain ratio.[79,80]

Shear wave imaging is dynamic elastography imaging. Stress is induced either by mechanical vibrator (transient elastography and MRE) or acoustic radiation force impulse (point shear wave elastography [SWE] and 2D SWE).[79,80] The velocity of generated shear waves inside the tissue is measured using Young's modulus E in m/s or kilopascal (kPa).

Various parameters can be measured to assess the mechanical property of a tissue, such as Young's modulus, viscosity, anisotrophy, and heterogeneity indices, and others. However, a simplified parameter, that is, Young's modulus, is sufficient for most practical purposes. The Young's modulus (E), also known as the shear elastic modulus (μ),is described by the terms "elasticity," "stiffness," or "hardness" which correspond to manual palpation.

The basic principle is to induce a motion or a deformation in the tissue by an external force and observing how the tissue responds during the tissue motion and consequently inferring the mechanical property of the tissue.[81]

The most important aspect of elastography is to measure the response or strain of the tissue to shear waves.

Techniques used for liver stiffness assessment are SWE and listed below:

- One-dimensional transient elastography (Fibro scan) uses mechanical vibrator which is in built in the probe itself to create dynamic stress at the body surface with frequency of 40 to 50 Hz for less than 30 seconds which leads to formation of shear waves and velocity of generated shear waves is measured using Young's modulus E without B-mode imaging.[82,83] It also provides fat quantification. However, it lacks morphologic imaging.

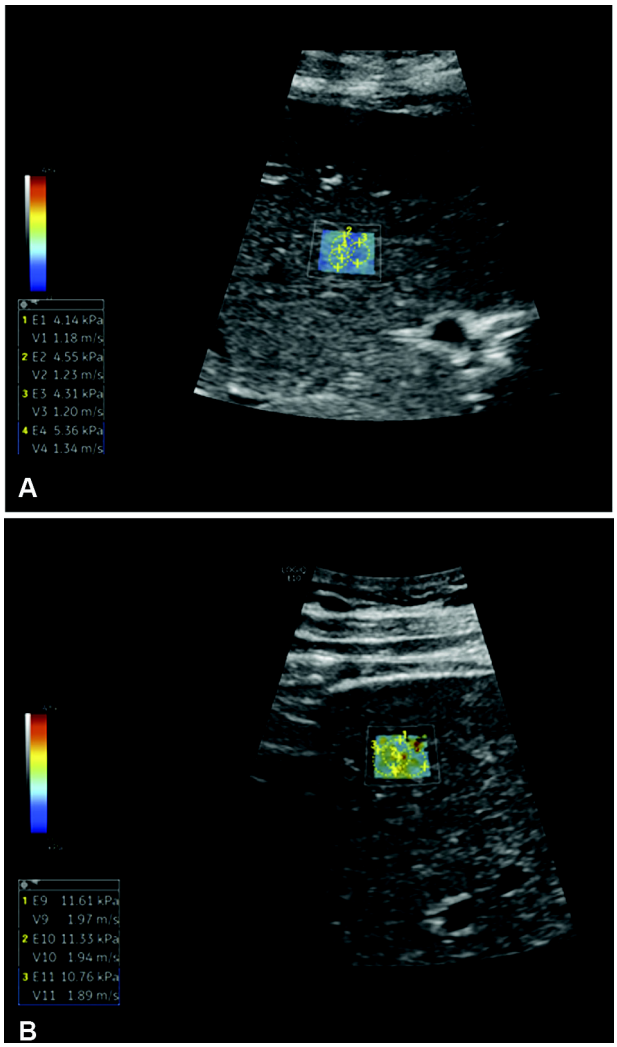

Fig. 17 Ultrasound elastography. (**a**) 2D shear wave elastography (SWE) demonstrates normal elastogram (color box) with mean kPa of 4.5. (**b**) 2D SWE demonstrates increased stiffness (color box) elastogram with mean kPa of 11. 2D, two-dimensional.

- Point SWE uses acoustic radiation force impulse (ARFI) to create dynamic stress in liver tissue to produce shear wave and velocity of this shear wave is measured using Young's modulus E using real-time imaging[84] on conventional ultrasound machine with curvilinear probe.[85] Body habitus and ascites are limitations for transient elastography as shear waves are produced by the stress induced at body surface; however, SWE overcomes these limitations by producing shear waves deep in the liver parenchyma itself. Moreover, in SWE technique, ROI can be targeted using real-time imaging in the region free of bile ducts and vessels.[80,86,87]
- SWE technique is the most recent and fastest ultrasound shear wave technique. In this technique, color map of shear wave can be seen superimposed over gray scale imaging in real time by producing cone-shaped beam of shear wave using multifocal ARFI induction (►**Fig. 17**). Velocity of shear wave is measured using Young's Modulus E.[84,88] The major drawback of this technique is its availability and validation.[89–91]
- MRE is a dynamic imaging technique which combines MR imaging with mechanical shear waves to create a stiffness map (elastogram) of the body tissues. Currently, MRE is used to determine the extent of liver fibrosis. It is can detect fibrosis in all stages and is reproducible and standard across vendors. It is superior to other elastography techniques.[78] MRE has a higher technical success rate than ultrasound elastography and a better diagnostic accuracy than ultrasound elastography for staging liver fibrosis.[92]

In a patient with chronic liver disease, one of the most important prognostic factor is whether or not the patient has cirrhosis. Hence, fibrosis staging systems can help to predict clinical outcomes in liver disease.[86,93] The diagnosis of decompensated liver cirrhosis can be assigned clinically by the presence of complications such as ascites, variceal hemorrhage, jaundice, and/or encephalopathy. It is the diagnosis of compensated cirrhosis that is more challenging. Radiological findings, such as a nodular liver surface, altered lobar anatomy, signs of portal hypertension, and others, that indicate the presence of cirrhosis are often absent in a patient with compensated cirrhosis; thus, a noninvasive study to confirm or exclude the presence of cirrhosis is needed.

The main indication for MRE is staging of fibrosis in chronic liver disease. Other indications for liver elastography include follow-up of previously diagnosed fibrosis, assessment of patients with known cirrhosis and evaluation of patients with unexplained portal hypertension. Another indication is follow-up assessment of treatment response and tailor further follow-up and therapy. Newer treatments can actually decrease fibrosis in patients with viral hepatitis. A study performed in patients with Hepatitis B Virus (HBV) infection who were undergoing antiviral therapy showed that histologic regression of fibrosis occurred in 91% of them, with cirrhosis regression occurring in 74% of patients after 5 years of therapy.[94,95]

Technique

MRE uses mechanical waves, typically shear waves, to quantify the stiffness of tissues. These shear waves are produced by a device called an "active acoustic driver." Active driver contains a "voice coil" suspended under a magnetic field. Passage of current through the voice coil under a magnetic field generates a force, called "Lorentz force" which ultimately produces vibrations. The fact that the active driver contains its own magnet, it has to be kept outside the MRI room. The vibrations produced by the active driver is mechanically transferred to another device called the "Passive driver" through a plastic tube. The passive driver is attached tightly over the abdomen, preferably over the right lobe of liver to cover a larger portion of the liver (►**Fig. 18A**).

The liver stiffness in healthy patients does not change significantly with food intake. However, in persons with chronic liver disease, liver stiffness may increase for a short time after a meal. For this reason, patient fasting for 4 to 6 hours before the MRE examination is recommended.[96–101]

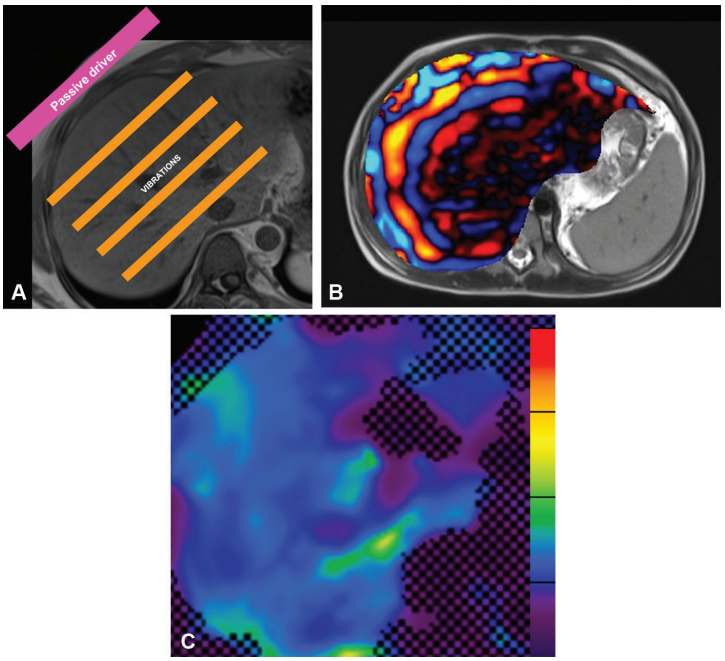

Fig. 18 MR elastography acquisition. (**A**) Demonstrates "passive driver" on the abdominal wall generating acoustic vibrations. (**B**) Demonstrates "wave formation" synchronized to the mechanical waves produce by the vibrations using a motion sensitive gradient sequence. (**C**) Color demonstrates stiffness map from 0 to 8 kPa. Purple color represents normal liver and stiffness and red color represents fibrosis and stiff liver. MR, magnetic resonance.

A typical MRE pulse sequence combines a gradient recalled echo (GRE) sequence with the conventional RF pulse waveform, slice-selection gradient, phase-encoding gradient, and frequency-encoding gradient. The motion-encoding gradient (MEG) is placed after the RF excitation of the sample and before the measurement of the induced signal. An MR image thus obtained containing information about the propagating wave in its phase is called a wave image (►**Fig. 18B**). Two wave images are obtained using opposite polarity of the MEG to create a phase difference image.[102,103]

Inversion algorithms are applied to the wave images that contain the information on the propagating shear waves.[104] The algorithms assume tissue as a linear, isotropic, homogeneous, and viscoelastic medium that allows calculation of the shear modulus. The maps which are produced with this are called stiffness maps or elastograms (►**Fig. 18C**). The color maps produce an overview of the stiffness inside the liver. The distribution of stiffness in the cross-section of the liver

Table 3 Interpretation of liver stiffness with MRE

Suggested guidelines for interpretation of liver stiffness with MRE at 60 Hz[78] (Venkatesh and Ehman)
<2.5 kPa: normal
2.5–2.9 kPa: normal or inflammation
2.9–3.5 kPa: stage 1 to 2 fibrosis
3.5–4 kPa: stages 2 and 3 fibrosis
4–5 kPa: stages 3 to 4 fibrosis
>5 kPa: stage-4 fibrosis or cirrhosis

Abbreviation: MRE, magnetic resonance elastography.

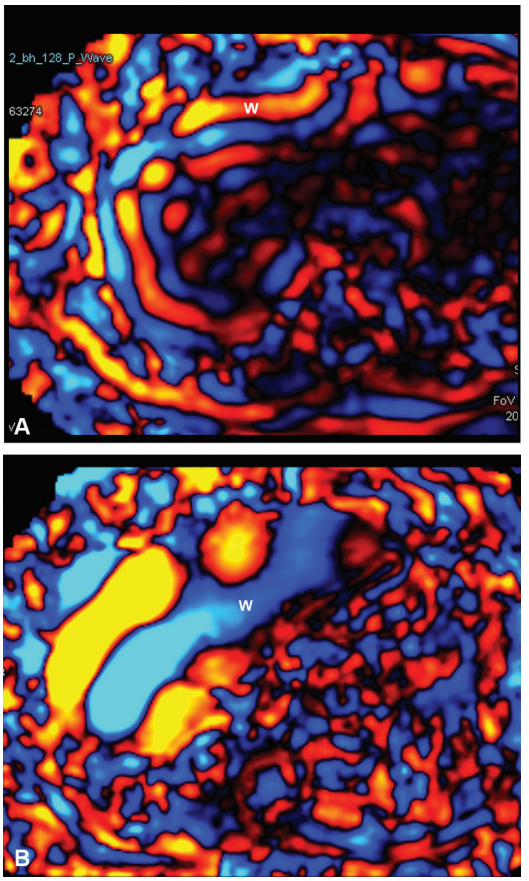

Fig. 19 MR elastography—wave image and liver stiffness. (**A**) MR elastography, wave image acquired at 60 MHz demonstrates the normal thickness of the waves (W), suggesting normal stiffness. (**B**) MR elastography, wave image acquired at 60 MHz demonstrates the increased thickness of the waves (W), suggesting a longer wavelength & a marker for increased stiffness. MR, magnetic resonance.

can be well seen on these color maps. In general, a scaled color map of 0 to 8 kPa suffices for routine clinical use.[78] ROI or segmentation value is created for quantification of kPa values. Various cut-offs are used and the most commonly used is described in ►**Table 3**.

Magnetic Resonance Elastography Interpretation

Shear waves used in MRE behave much like sound waves. It travels farther in the stiff media and gets attenuated in an elastic one.

In a normal healthy liver, the liver parenchyma is soft. Hence, the shear waves are attenuated more as compared with a fibrotic liver. This results in thin waves which attenuate centrally. In a fibrotic liver, we get thicker waves which are less attenuated centrally[96] (►**Fig. 19**).

Role of Magnetic Resonance Elastography in Hepatic Steatosis

According to study conducted by Yin et al, the liver stiffness does not appear to be influenced by the degree of steatosis. Liver stiffness increases systematically with fibrosis stage.[105]

It is an effective, noninvasive method to detect and grade the degree of hepatic fibrosis in NAFLD. This method has good accuracy in differentiating a normal subject from NAFLD subjects and between the mild, moderate, and severe grades of fibrosis. NAFLD patients with inflammation and without fibrosis have higher liver stiffness than those with

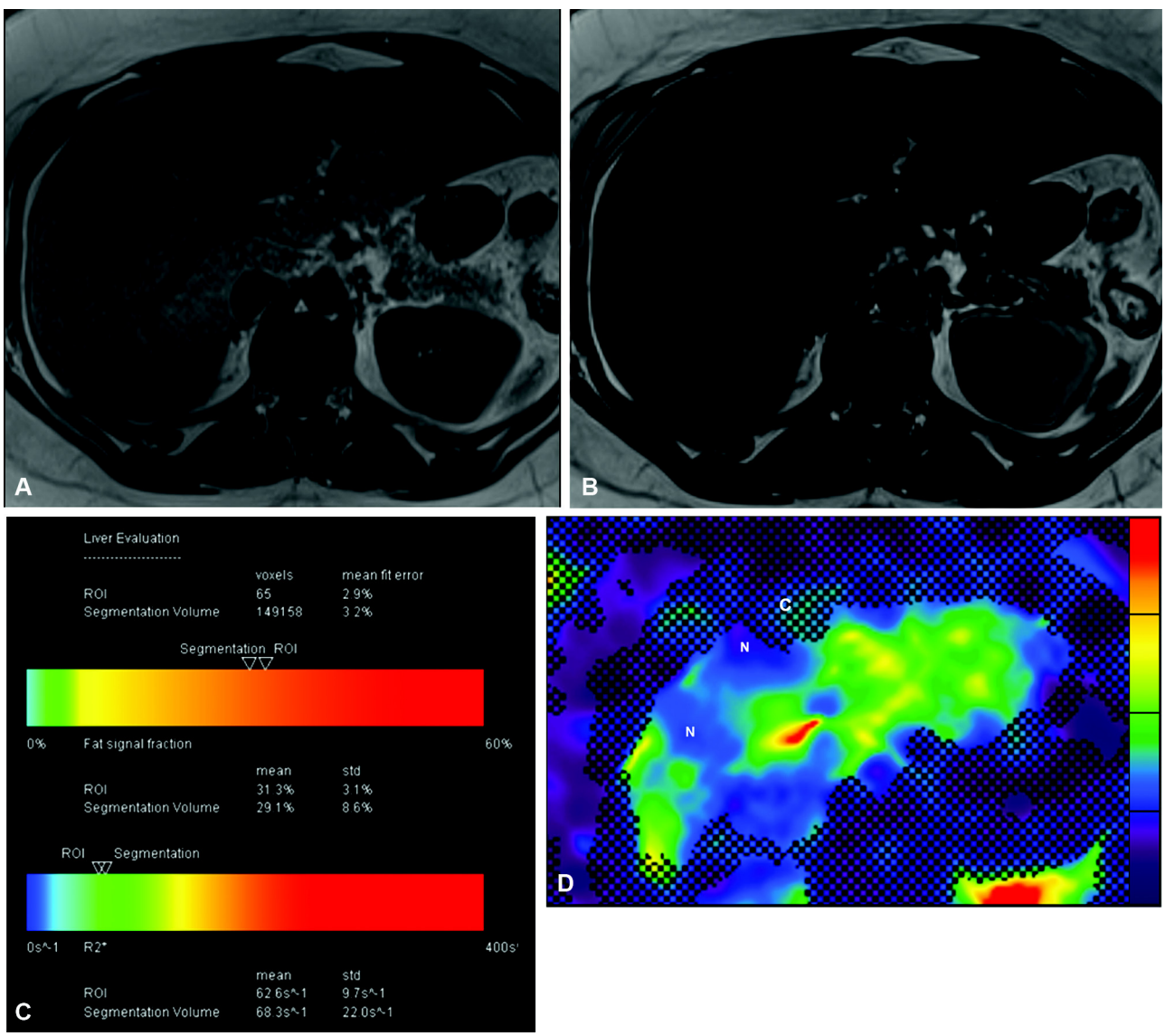

Fig. 20 NASH and MR elastography. (**A**) GRE T1-weighted in-phase demonstrates liver to be brighter than usual. (**B**) GRE T1-weighted out-phase demonstrates significant signal drop, suggesting severe fatty accumulation. (**C**) The color bar shows the value of PDFF (top bar) and R2* (bottom bar). Both ROI (31%) and segmentation (29%) demonstrate significant and diffuse fat accumulation. The R2* value in the lower bar demonstrates mild iron deposition. (**D**) Color elastogram with a 0–8 kPa demonstrates stiffness distribution. Note there is heterogeneity with varying grades of fibrosis. The side color bar denotes red color as grade-IV fibrosis and blue-purple as normal (grade-0 fibrosis). This is suggestive of inflammation with early fibrosis and is reversible at this stage. NASH, nonalcoholic steatohepatitis; PDFF, proton density fat fraction; ROI, region of interest.

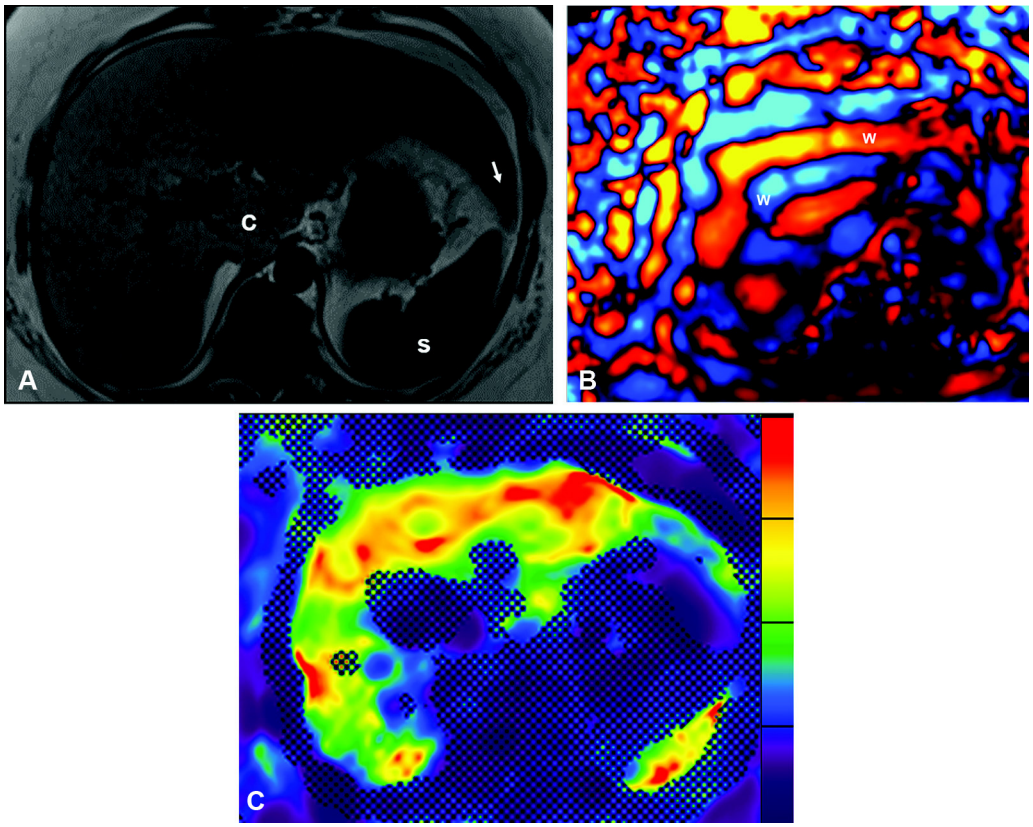

Fig. 21 Liver cirrhosis and MR elastography. (**A**) GRE T1-weighted "in-phase" image in axial plane demonstrates the liver to be brighter than usual and has altered lobar anatomy. The caudate lobe (**B**) is enlarged and the left lobe show enlargement toward the spleen (white arrow). Please note the surface is not nodular. (**C**) MR elastography, wave image acquired at 60 MHz demonstrates thick waves (W), suggesting longer wavelength of the shear waves and a mark for increased stiffness. (**D**) MR elastogram, with a 0–8 kPa demonstrates stiffness distribution. The degree of fibrosis is in the grade-III/IV category. The side color bar denotes red color as grade-IV fibrosis and yellow color as grade-III fibrosis. MR, magnetic resonance.

simple steatosis (►**Fig. 20**). In advanced cirrhosis grade-4 fibrosis is seen (►**Fig. 21**). There are significant associations between liver stiffness and nonalcoholic steatosis even in the absence of hepatic fibrosis which indicates a possible effect of inflammation on liver stiffness.[105,106] MRE can be used for follow-up to assess the response to the treatment (►**Fig. 22**).

Other Causes of Raised Liver Stiffness/Conditions Mimicking Fibrosis

Liver stiffness values will increase after a meal, especially in patients with chronic liver disease. Therefore, patients should fast 4 to 6 hours before undergoing liver MRE.[97,98,100]

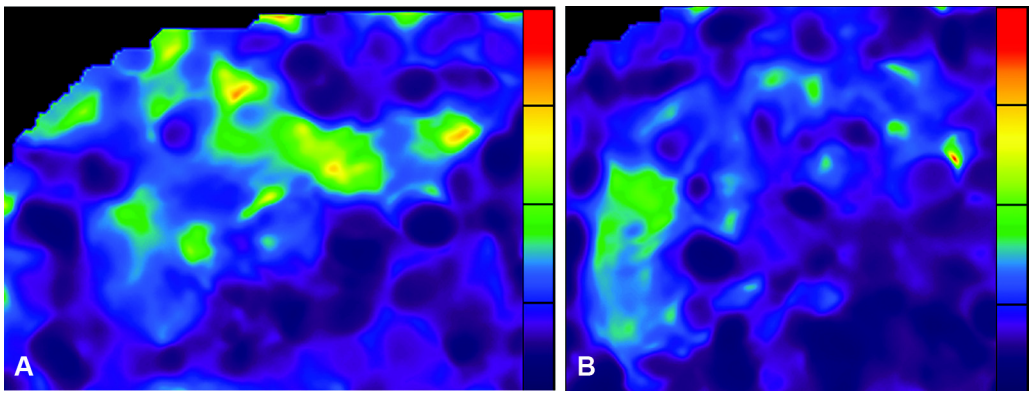

Fig. 22 NASH reversal of liver early fibrosis on therapy. (**A**) Color elastogram with a 0–8 kPa demonstrates stiffness distribution. Note there is heterogeneity with varying levels of fibrosis. The side color bar denotes red color as grade-IV fibrosis and blue-purple as normal. This image represents early and patchy fibrosis. (**B**) Follow-up scan after 2 years following medical therapy. Color elastogram with a 0–8 kPa demonstrates stiffness distribution. Note there is improvement in the stiffness levels, suggesting a response to therapy. NASH, nonalcoholic steatohepatitis.

Other causes which can mimic fibrosis include acute inflammation, extrahepatic cholestasis, hepatic congestion, and infiltrative processes.[107,108]

Since causes other than fibrosis or cirrhosis can lead to increased liver stiffness measurement (LSMs), the measurements should always be interpreted in conjunction with clinical and laboratory findings for other possible causes of the increased liver stiffness.[96]

Conclusion

Fatty liver is essentially a benign condition; however, longstanding hepatic steatosis can lead to inflammation resulting into NASH and progressive fibrosis with end result being cirrhosis and increased incidence of hepatocellular carcinoma. Early stages of fibrosis in the liver is reversible and the radiologist can play a vital role in detecting the fat, quantifying it, detecting early signs of chronic liver disease, and fibrosis. PDFF is surrogate marker for fat in the liver, while MRE is surrogate marker for fibrosis in the liver.

Conflict of Interest
None declared.

References

1 Ahmed MH, Barakat S, Almobarak AO. Nonalcoholic fatty liver disease and cardiovascular disease: has the time come for cardiologists to be hepatologists? J Obes 2012;2012:483135
2 Loomba R, Sanyal AJ. The global NAFLD epidemic. Nat Rev Gastroenterol Hepatol 2013;10(11):686–690
3 De A, Duseja A. Nonalcoholic fatty liver disease: Indian perspective. Clin Liver Dis (Hoboken) 2021;18(03):158–163
4 Marchesini G, Bugianesi E, Forlani G, et al. Nonalcoholic fatty liver, steatohepatitis, and the metabolic syndrome. Hepatology 2003;37(04):917–923
5 Manne V, Handa P, Kowdley KV. Pathophysiology of nonalcoholic fatty liver disease/nonalcoholic steatohepatitis. Clin Liver Dis 2018;22(01):23–37
6 Wang Y, Rimm EB, Stampfer MJ, Willett WC, Hu FB. Comparison of abdominal adiposity and overall obesity in predicting risk of type 2 diabetes among men. Am J Clin Nutr 2005;81(03): 555–563
7 Kral JG, Lundholm K, Björntorp P, Sjöström L, Scherstén T. Hepatic lipid metabolism in severe human obesity. Metabolism 1977;26(09):1025–1031
8 Sanyal AJ, Campbell-Sargent C, Mirshahi F, et al. Nonalcoholic steatohepatitis: association of insulin resistance and mitochondrial abnormalities. Gastroenterology 2001;120(05): 1183–1192
9 Basaranoglu M, Basaranoglu G, Bugianesi E. Carbohydrate intake and nonalcoholic fatty liver disease: fructose as a weapon of mass destruction. Hepatobiliary Surg Nutr 2015;4(02):109–116
10 Marra F, Tacke F. Roles for chemokines in liver disease. Gastroenterology 2014;147(03):577–594.e1
11 Pritchard MT, McCracken JM. Identifying novel targets for treatment of liver fibrosis: what can we learn from injured tissues which heal without a scar? Curr Drug Targets 2015;16(12): 1332–1346
12 Hamer OW, Aguirre DA, Casola G, Lavine JE, Woenckhaus M, Sirlin CB. Fatty liver: imaging patterns and pitfalls. Radiographics 2006;26(06):1637–1653
13 Valls C, Iannacconne R, Alba E, et al. Fat in the liver: diagnosis and characterization. Eur Radiol 2006;16(10):2292–2308
14 Schwenzer NF, Springer F, Schraml C, Stefan N, Machann J, Schick F. Non-invasive assessment and quantification of liver steatosis by ultrasound, computed tomography and magnetic resonance. J Hepatol 2009;51(03):433–445
15 Brunt EM. Pathology of fatty liver disease. Mod Pathol 2007;20 (Suppl 1):S40–S48
16 Maharaj B, Maharaj RJ, Leary WP, et al. Sampling variability and its influence on the diagnostic yield of percutaneous needle biopsy of the liver. Lancet 1986;1(8480):523–525
17 Arun J, Jhala N, Lazenby AJ, Clements R, Abrams GA. Influence of liver biopsy heterogeneity and diagnosis of nonalcoholic steatohepatitis in subjects undergoing gastric bypass. Obes Surg 2007;17(02):155–161
18 Chen C-L, Cheng Y-F, Yu C-Y, et al. Living donor liver transplantation: the Asian perspective. Transplantation 2014;97(Suppl 8): S3
19 Chartampilas E. Imaging of nonalcoholic fatty liver disease and its clinical utility. Hormones (Athens) 2018;17(01):69–81
20 Charatcharoenwitthaya P, Lindor KD. Role of radiologic modalities in the management of non-alcoholic steatohepatitis. Clin Liver Dis 2007;11(01):37–54, viii
21 Saadeh S, Younossi ZM, Remer EM, et al. The utility of radiological imaging in nonalcoholic fatty liver disease. Gastroenterology 2002;123(03):745–750
22 Strauss S, Gavish E, Gottlieb P, Katsnelson L. Interobserver and intraobserver variability in the sonographic assessment of fatty liver. AJR Am J Roentgenol 2007;189(06):W320-3
23 Lee SS, Park SH. Radiologic evaluation of nonalcoholic fatty liver disease. World J Gastroenterol 2014;20(23):7392–7402
24 Kodama Y, Ng CS, Wu TT, et al. Comparison of CT methods for determining the fat content of the liver. AJR Am J Roentgenol 2007;188(05):1307–1312
25 Joy D, Thava VR, Scott BB. Diagnosis of fatty liver disease: is biopsy necessary? Eur J Gastroenterol Hepatol 2003;15(05): 539–543
26 Piekarski J, Goldberg HI, Royal SA, Axel L, Moss AA. Difference between liver and spleen CT numbers in the normal adult: its usefulness in predicting the presence of diffuse liver disease. Radiology 1980;137(03):727–729
27 Limanond P, Raman SS, Lassman C, et al. Macrovesicular hepatic steatosis in living related liver donors: correlation between CT and histologic findings. Radiology 2004;230(01):276–280
28 Hamer OW, Aguirre DA, Casola G, Sirlin CB. Imaging features of perivascular fatty infiltration of the liver: initial observations. Radiology 2005;237(01):159–169
29 Pamilo M, Sotaniemi EA, Suramo I, Lähde S, Arranto AJ. Evaluation of liver steatotic and fibrous content by computerized tomography and ultrasound. Scand J Gastroenterol 1983;18 (06):743–747
30 Yajima Y, Narui T, Ishii M, et al. Computed tomography in the diagnosis of fatty liver: total lipid content and computed tomography number. Tohoku J Exp Med 1982;136(03):337–342
31 Park SH, Kim PN, Kim KW, et al. Macrovesicular hepatic steatosis in living liver donors: use of CT for quantitative and qualitative assessment. Radiology 2006;239(01):105–112
32 Kawamoto S, Soyer PA, Fishman EK, Bluemke DA. Nonneoplastic liver disease: evaluation with CT and MR imaging. Radiographics 1998;18(04):827–848
33 Rofsky NM, Fleishaker H. CT and MRI of diffuse liver disease. Semin Ultrasound CT MR 1995;16(01):16–33
34 Kinner S, Reeder SB, Yokoo T. Quantitative Imaging Biomarkers of NAFLD. Dig Dis Sci 2016;61(05):1337–1347
35 Girometti R. 3.0 Tesla magnetic resonance imaging: A new standard in liver imaging? World J Hepatol 2015;7(15): 1894–1898
36 Huber A, Ebner L, Montani M, et al. Computed tomography findings in liver fibrosis and cirrhosis. Accessed January 12, 2022 at: https://smw.ch/article/doi/smw.2014.13923

37 Qayyum A, Goh JS, Kakar S, Yeh BM, Merriman RB, Coakley FV. Accuracy of liver fat quantification at MR imaging: comparison of out-of-phase gradient-echo and fat-saturated fast spin-echo techniques–initial experience. Radiology 2005;237(02): 507–511
38 Dixon WT. Simple proton spectroscopic imaging. Radiology 1984;153(01):189–194
39 Ma J. Dixon techniques for water and fat imaging. J Magn Reson Imaging 2008;28(03):543–558
40 Reeder SB, Cruite I, Hamilton G, Sirlin CB. Quantitative assessment of liver fat with magnetic resonance imaging and spectroscopy. J Magn Reson Imaging 2011;34(04):729–749
41 Outwater EK, Blasbalg R, Siegelman ES, Vala M. Detection of lipid in abdominal tissues with opposed-phase gradient-echo images at 1.5 T: techniques and diagnostic importance. Radiographics 1998;18(06):1465–1480
42 Bley TA, Wieben O, François CJ, Brittain JH, Reeder SB. Fat and water magnetic resonance imaging. J Magn Reson Imaging 2010; 31(01):4–18
43 Reeder SB, Pineda AR, Wen Z, et al. Iterative decomposition of water and fat with echo asymmetry and least-squares estimation (IDEAL): application with fast spin-echo imaging. Magn Reson Med 2005;54(03):636–644
44 Liu C-Y, McKenzie CA, Yu H, Brittain JH, Reeder SB. Fat quantification with IDEAL gradient echo imaging: correction of bias from T(1) and noise. Magn Reson Med 2007;58(02): 354–364
45 Bydder M, Yokoo T, Hamilton G, et al. Relaxation effects in the quantification of fat using gradient echo imaging. Magn Reson Imaging 2008;26(03):347–359
46 Yu H, McKenzie CA, Shimakawa A, et al. Multiecho reconstruction for simultaneous water-fat decomposition and T2* estimation. J Magn Reson Imaging 2007;26(04):1153–1161
47 Yu H, Shimakawa A, McKenzie CA, Brodsky E, Brittain JH, Reeder SB. Multiecho water-fat separation and simultaneous R2* estimation with multifrequency fat spectrum modeling. Magn Reson Med 2008;60(05):1122–1134
48 Reeder SB, Hu HH, Sirlin CB. Proton density fat-fraction: a standardized MR-based biomarker of tissue fat concentration. J Magn Reson Imaging 2012;36(05):1011–1014
49 Henninger B, Alustiza J, Garbowski M, Gandon Y. Practical guide to quantification of hepatic iron with MRI. Eur Radiol 2020;30 (01):383–393
50 Procter AJ, Sun JY, Malcolm PN, Toms AP. Measuring liver fat fraction with complex-based chemical shift MRI: the effect of simplified sampling protocols on accuracy. BMC Med Imaging 2019;19(01):14
51 Caussy C, Reeder SB, Sirlin CB, Loomba R. Noninvasive, quantitative assessment of liver fat by MRI-PDFF as an endpoint in NASH trials. Hepatology 2018;68(02):763–772
52 Idilman IS, Aniktar H, Idilman R, et al. Hepatic steatosis: quantification by proton density fat fraction with MR imaging versus liver biopsy. Radiology 2013;267(03):767–775
53 Bannas P, Kramer H, Hernando D, et al. Quantitative magnetic resonance imaging of hepatic steatosis: validation in ex vivo human livers. Hepatology 2015;62(05):1444–1455
54 Dennis A, Kelly MD, Fernandes C, et al. Correlations between MRI biomarkers PDFF and cT1 with histopathological features of non-alcoholic steatohepatitis. Front Endocrinol (Lausanne) 2021; 11:575843
55 Permutt Z, Le T-A, Peterson MR, et al. Correlation between liver histology and novel magnetic resonance imaging in adult patients with non-alcoholic fatty liver disease - MRI accurately quantifies hepatic steatosis in NAFLD. Aliment Pharmacol Ther 2012;36(01):22–29
56 Kleiner DE, Brunt EM, Van Natta M, et al; Nonalcoholic Steatohepatitis Clinical Research Network. Design and validation of a histological scoring system for nonalcoholic fatty liver disease. Hepatology 2005;41(06):1313–1321
57 Tang A, Tan J, Sun M, et al. Nonalcoholic fatty liver disease: MR imaging of liver proton density fat fraction to assess hepatic steatosis. Radiology 2013;267(02):422–431
58 Caussy C, Alquiraish MH, Nguyen P, et al. Optimal threshold of controlled attenuation parameter with MRI-PDFF as the gold standard for the detection of hepatic steatosis. Hepatology 2018; 67(04):1348–1359
59 Tang A, Desai A, Hamilton G, et al. Accuracy of MR imaging-estimated proton density fat fraction for classification of dichotomized histologic steatosis grades in nonalcoholic fatty liver disease. Radiology 2015;274(02):416–425
60 Dulai PS, Sirlin CB, Loomba R. MRI and MRE for non-invasive quantitative assessment of hepatic steatosis and fibrosis in NAFLD and NASH: Clinical trials to clinical practice. J Hepatol 2016;65(05):1006–1016
61 Tyagi A, Yeganeh O, Levin Y, et al. Intra- and inter-examination repeatability of magnetic resonance spectroscopy, magnitude-based MRI, and complex-based MRI for estimation of hepatic proton density fat fraction in overweight and obese children and adults. Abdom Imaging 2015;40(08):3070–3077
62 Negrete LM, Middleton MS, Clark L, et al. Inter-examination precision of magnitude-based MRI for estimation of segmental hepatic proton density fat fraction in obese subjects. J Magn Reson Imaging 2014;39(05):1265–1271
63 Kang GH, Cruite I, Shiehmorteza M, et al. Reproducibility of MRI-determined proton density fat fraction across two different MR scanner platforms. J Magn Reson Imaging 2011;34(04):928–934
64 Artz NS, Haufe WM, Hooker CA, et al. Reproducibility of MR-based liver fat quantification across field strength: Same-day comparison between 1.5T and 3T in obese subjects. J Magn Reson Imaging 2015;42(03):811–817
65 Athithan L, Gulsin GS, House MJ, et al. A comparison of liver fat fraction measurement on MRI at 3T and 1.5T. PLoS One 2021;16 (07):e0252928
66 Noureddin M, Lam J, Peterson MR, et al. Utility of magnetic resonance imaging versus histology for quantifying changes in liver fat in nonalcoholic fatty liver disease trials. Hepatology 2013;58(06):1930–1940
67 Loomba R, Sirlin CB, Ang B, et al; San Diego Integrated NAFLD Research Consortium (SINC) Ezetimibe for the treatment of nonalcoholic steatohepatitis: assessment by novel magnetic resonance imaging and magnetic resonance elastography in a randomized trial (MOZART trial). Hepatology 2015;61(04): 1239–1250
68 Patel J, Bettencourt R, Cui J, et al. Association of noninvasive quantitative decline in liver fat content on MRI with histologic response in nonalcoholic steatohepatitis. Therap Adv Gastroenterol 2016;9(05):692–701
69 Harrison SA, Bashir MR, Guy CD, et al. Resmetirom (MGL-3196) for the treatment of non-alcoholic steatohepatitis: a multicentre, randomised, double-blind, placebo-controlled, phase 2 trial. Lancet 2019;394(10213):2012–2024
70 Harrison SA, Rossi SJ, Paredes AH, et al. NGM282 improves liver fibrosis and histology in 12 weeks in patients with nonalcoholic steatohepatitis. Hepatology 2020;71(04):1198–1212
71 Le T-A, Chen J, Changchien C, et al; San Diego Integrated NAFLD Research Consortium (SINC) Effect of colesevelam on liver fat quantified by magnetic resonance in nonalcoholic steatohepatitis: a randomized controlled trial. Hepatology 2012;56(03):922–932
72 Doycheva I, Cui J, Nguyen P, et al. Non-invasive screening of diabetics in primary care for NAFLD and advanced fibrosis by MRI and MRE. Aliment Pharmacol Ther 2016;43(01):83–95
73 Hamilton G, Yokoo T, Bydder M, et al. In vivo characterization of the liver fat ^{1}H MR spectrum. NMR Biomed 2011;24(07): 784–790

74 Meisamy S, Hines CDG, Hamilton G, et al. Quantification of hepatic steatosis with T1-independent, T2-corrected MR imaging with spectral modeling of fat: blinded comparison with MR spectroscopy. Radiology 2011;258(03):767–775

75 Heba ER, Desai A, Zand KA, et al. Accuracy and the effect of possible subject-based confounders of magnitude-based MRI for estimating hepatic proton density fat fraction in adults, using MR spectroscopy as reference. J Magn Reson Imaging 2016;43 (02):398–406

76 Bastati N, Feier D, Wibmer A, et al. Noninvasive differentiation of simple steatosis and steatohepatitis by using gadoxetic acid-enhanced MR imaging in patients with nonalcoholic fatty liver disease: a proof-of-concept study. Radiology 2014;271(03):739–747

77 Smits LP, Coolen BF, Panno MD, et al. Noninvasive differentiation between hepatic steatosis and steatohepatitis with MR imaging enhanced with USPIOs in patients with nonalcoholic fatty liver disease: a proof-of-concept study. Radiology 2016;278(03):782–791

78 Venkatesh SK, Ehman RL. Magnetic resonance elastography of liver. Magn Reson Imaging Clin N Am 2014;22(03):433–446

79 Sigrist RMS, Liau J, Kaffas AE, Chammas MC, Willmann JK. Ultrasound elastography: review of techniques and clinical applications. Theranostics 2017;7(05):1303–1329

80 Tang A, Cloutier G, Szeverenyi NM, Sirlin CB. Ultrasound elastography and MR elastography for assessing liver fibrosis: part 1, principles and techniques. AJR Am J Roentgenol 2015;205(01): 22–32

81 Lu J, Chen M, Chen Q-H, Wu Q, Jiang J-N, Leung T-Y. Elastogram: physics, clinical applications, and risks. Maternal-Fetal Medicine. 2019;1:113–122

82 Dhyani M, Anvari A, Samir AE. Ultrasound elastography: liver. Abdom Imaging 2015;40(04):698–708

83 Audière S, Angelini ED, Sandrin L, Charbit M. Maximum likelihood estimation of shear wave speed in transient elastography. IEEE Trans Med Imaging 2014;33(06):1338–1349

84 Bamber J, Cosgrove D, Dietrich CF, et al. EFSUMB guidelines and recommendations on the clinical use of ultrasound elastography. Part 1: Basic principles and technology. Ultraschall Med 2013;34 (02):169–184

85 Friedrich-Rust M, Nierhoff J, Lupsor M, et al. Performance of acoustic radiation force impulse imaging for the staging of liver fibrosis: a pooled meta-analysis. J Viral Hepat 2012;19(02):e212–e219

86 Barr RG, Ferraioli G, Palmeri ML, et al. Elastography assessment of liver fibrosis: Society of Radiologists in Ultrasound Consensus Conference Statement. Radiology 2015;276(03):845–861

87 Morikawa H, Fukuda K, Kobayashi S, et al. Real-time tissue elastography as a tool for the noninvasive assessment of liver stiffness in patients with chronic hepatitis C. J Gastroenterol 2011;46(03):350–358

88 Cosgrove D, Piscaglia F, Bamber J, et al; EFSUMB. EFSUMB guidelines and recommendations on the clinical use of ultrasound elastography. Part 2: clinical applications. Ultraschall Med 2013; 34(03):238–253

89 Muller M, Gennisson J-L, Deffieux T, Tanter M, Fink M. Quantitative viscoelasticity mapping of human liver using supersonic shear imaging: preliminary in vivo feasibility study. Ultrasound Med Biol 2009;35(02):219–229

90 Ferraioli G, Tinelli C, Dal Bello B, Zicchetti M, Filice G, Filice CLiver Fibrosis Study Group. Accuracy of real-time shear wave elastography for assessing liver fibrosis in chronic hepatitis C: a pilot study. Hepatology 2012;56(06):2125–2133

91 Yoon JH, Lee JM, Joo I, et al. Hepatic fibrosis: prospective comparison of MR elastography and US shear-wave elastography for evaluation. Radiology 2014;273(03):772–782

92 Huwart L, Sempoux C, Vicaut E, et al. Magnetic resonance elastography for the noninvasive staging of liver fibrosis. Gastroenterology 2008;135(01):32–40

93 European Association For The Study Of The Liver. EASL clinical practice guidelines: management of chronic hepatitis B virus infection. J Hepatol 2012;57(01):167–185

94 Carrión JA, Navasa M, García-Retortillo M, et al. Efficacy of antiviral therapy on hepatitis C recurrence after liver transplantation: a randomized controlled study. Gastroenterology 2007; 132(05):1746–1756

95 Marcellin P, Gane E, Buti M, et al. Regression of cirrhosis during treatment with tenofovir disoproxil fumarate for chronic hepatitis B: a 5-year open-label follow-up study. Lancet 2013;381 (9865):468–475

96 Guglielmo FF, Venkatesh SK, Mitchell DG. Liver MR elastography technique and image interpretation: pearls and pitfalls. Radiographics 2019;39(07):1983–2002

97 Kennedy P, Wagner M, Castéra L, et al. Quantitative elastography methods in liver disease: current evidence and future directions. Radiology 2018;286(03):738–763

98 Jajamovich GH, Dyvorne H, Donnerhack C, Taouli B. Quantitative liver MRI combining phase contrast imaging, elastography, and DWI: assessment of reproducibility and postprandial effect at 3.0 T. PLoS One 2014;9(05):e97355

99 Berzigotti A, De Gottardi A, Vukotic R, et al. Effect of meal ingestion on liver stiffness in patients with cirrhosis and portal hypertension. PLoS One 2013;8(03):e58742

100 Hines CDG, Lindstrom MJ, Varma AK, Reeder SB. Effects of postprandial state and mesenteric blood flow on the repeatability of MR elastography in asymptomatic subjects. J Magn Reson Imaging 2011;33(01):239–244

101 Mederacke I, Wursthorn K, Kirschner J, et al. Food intake increases liver stiffness in patients with chronic or resolved hepatitis C virus infection. Liver Int 2009;29(10): 1500–1506

102 Mariappan YK, Glaser KJ, Ehman RL. Magnetic resonance elastography: a review. Clin Anat 2010;23(05):497–511

103 McCracken PJ, Manduca A, Felmlee J, Ehman RL. Mechanical transient-based magnetic resonance elastography. Magn Reson Med 2005;53(03):628–639

104 Manduca A, Oliphant TE, Dresner MA, et al. Magnetic resonance elastography: non-invasive mapping of tissue elasticity. Med Image Anal 2001;5(04):237–254

105 Yin M, Talwalkar JA, Glaser KJ, et al. Assessment of hepatic fibrosis with magnetic resonance elastography. Clin Gastroenterol Hepatol 2007;5(10):1207–1213.e2

106 Costa-Silva L, Ferolla SM, Lima AS, Vidigal PVT, Ferrari TCA. MR elastography is effective for the non-invasive evaluation of fibrosis and necroinflammatory activity in patients with nonalcoholic fatty liver disease. Eur J Radiol 2018;98:82–89

107 Millonig G, Reimann FM, Friedrich S, et al. Extrahepatic cholestasis increases liver stiffness (FibroScan) irrespective of fibrosis. Hepatology 2008;48(05):1718–1723

108 Pfeifer L, Strobel D, Neurath MF, Wildner D. Liver stiffness assessed by acoustic radiation force impulse (ARFI) technology is considerably increased in patients with cholestasis. Ultraschall Med 2014;35(04):364–367

